

Generalization in Graph Neural Networks: Improved PAC-Bayesian Bounds on Graph Diffusion

Haotian Ju^{*†}, Dongyue Li^{*†}, Aneesh Sharma^{*‡}, and Hongyang R. Zhang^{*†}

[†]*Northeastern University, Boston*

[‡]*Google, Mountain View*

Abstract

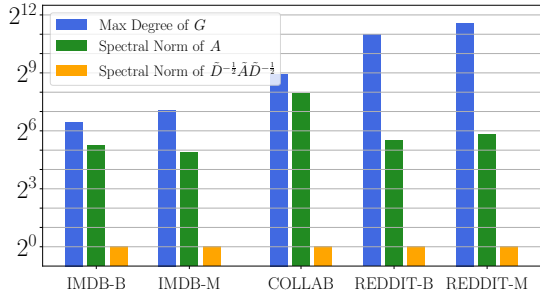
Graph neural networks are widely used tools for graph prediction tasks. Motivated by their empirical performance, prior works have developed generalization bounds for graph neural networks, which scale with graph structures in terms of the maximum degree. In this paper, we present generalization bounds that instead scale with the largest singular value of the graph neural network’s feature diffusion matrix. These bounds are numerically much smaller than prior bounds for real-world graphs. We also construct a lower bound of the generalization gap that matches our upper bound asymptotically. To achieve these results, we analyze a unified model that includes prior works’ settings (i.e., convolutional and message-passing networks) and new settings (i.e., graph isomorphism networks). Our key idea is to measure the stability of graph neural networks against noise perturbations using Hessians. Empirically, we find that Hessian-based measurements correlate with the observed generalization gaps of graph neural networks accurately. Optimizing noise stability properties for fine-tuning pretrained graph neural networks also improves test performance on several graph-level classification tasks.

1 Introduction

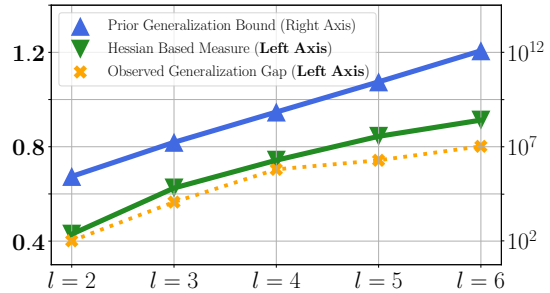
A central measure of success for a machine learning model is the ability to generalize well from training data to test data. For linear and shallow models, the generalization gap between their training performance and test performance can be quantified via complexity notions such as the Vapnik–Chervonenkis dimension and Rademacher complexity. However, formally explaining the empirical generalization performance of deep models remains a challenging problem and an active research area (see, e.g., recent textbook by Hardt and Recht [25]). There are by now many studies for fully-connected and convolutional neural networks that provide an explanation for their superior empirical performance [4, 44]. Our work seeks to formally understand generalization in graph neural networks (GNN) [46], which are commonly used for learning on graphs [23].

As a concrete example for motivating the study of generalization performance, we consider the fine-tuning of pretrained graph neural networks [27]. Given a pretrained GNN learned on a diverse range of graphs, fine-tuning the pretrained GNN on a specific prediction task is a common approach for transfer learning on graphs. An empirical problem with fine-tuning is that, on one hand, pretrained GNNs use lots of parameters to ensure representational power. On the other hand, fine-tuning a large GNN would overfit the training data and suffer poor test performance without

^{*}This is the arXiv version for a conference paper published in Artificial Intelligence and Statistics (AISTATS), 2023. Emails: {ju.h, li.dongyu, ho.zhang}@northeastern.edu and aneesh@google.com.



(a) Spectral norm vs. max degree for five graphs



(b) Comparing generalization bounds

Figure 1: The spectral norm bounds for graph diffusion matrices are orders of magnitude smaller than maximum degree bounds on real-world graphs; In Figure 1a, we measure the spectral norm and the max degree for five graph datasets. In Figure 1b, the Hessian-based generalization measure (plotted in green, scaled according to the *left axis*) matches the empirically observed generalization gaps of graph neural networks (plotted in yellow, scaled according to the *left axis*). The blue line shows a uniform-convergence bound (scaled according to the *right axis*) that is orders of magnitude larger than the observed gaps.

proper algorithmic intervention. Thus, a better understanding of generalization in graph neural networks can help us identify the cause of overfitting and, consequently, inspire designing robust fine-tuning methods for graph neural networks.

A naive application of the generalization bounds from fully-connected feedforward networks [4, 43] to GNNs would imply an extra term in the generalization bound that scales with n^{l-1} , where n is the number of nodes in the graph, hence rendering the error bounds vacuous. Besides, Scarselli et al. [47] shows that the VC dimension of GNN scales with n . Thus, although the VC dimension is a classical notion for deriving learning bounds, it is oblivious to the graph structure. Recent works have taken a step towards addressing this issue with better error analysis. Verma and Zhang (2019) find that one-layer graph neural networks satisfy uniform stability properties [50], following the work of Hardt et al. [26]. The generalization bound of Verma and Zhang [50] scales with the largest singular value of the graph diffusion matrix of the model. However, their analysis only applies to a single layer and node prediction. Garg et al. (2020) analyze an l layer message-passing neural network — with $l-1$ graph diffusion layers and 1 pooling layer — for graph prediction tasks [16]. Their result scales with d^{l-1} , where d is the maximum degree of the graph. Subsequently, Liao et al. (2021) develop a tighter bound but still scales with d^{l-1} [38]. For both results, the graph’s maximum degree is used to quantify the complexity of node aggregation in each diffusion step.

Our main contribution is to show generalization bounds for graph neural networks by reducing the max degree to the spectral norm of the graph diffusion matrix. We achieve this by analyzing the stability of a graph neural network against noise injections. To illustrate, denote an l -layer GNN by f . By PAC-Bayesian analysis [40], the generalization gap of f will be small if f remains stable against noise injections; otherwise, the generalization gap of f will be large. Empirically, quantifying the noise stability of f via Lipschitz-continuity properties of its activation functions leads to nonvacuous bounds for feedforward networks that correlate with their observed generalization gaps [12, 2, 31, 34]. Our theoretical analysis rigorously formalizes this with refined stability analysis of graph neural networks through Hessians, leading to tight generalization bounds on the graph diffusion matrix.

Our Contributions. The goal of this work is to improve the theoretical understanding of generalization in graph neural networks, and in that vein, we highlight two results below:

- First, we prove sharp generalization bounds for message-passing neural networks [9, 17, 33], graph convolutional networks [36], and graph isomorphism networks [55]. Our bounds scale with the spectral norm of P_G^{l-1} for an l -layer network, where P_G denotes a diffusion matrix on a graph G and varies between different models (see Theorem 3.1 for the full statement). We then show a matching lower bound instance where the generalization gap scales with the spectral norm of P_G^{l-1} (see Theorem 3.2).
- Second, our stability analysis of graph neural networks provides a practical tool for measuring generalization. Namely, we show that the trace of the loss Hessian matrix can measure the noise stability of GNN. The formal statement is given in Lemma 4.3, and our techniques, which include a uniform convergence of the Hessian matrix, may be of independent interest. We note that the proof applies to twice-differentiable and Lipschitz-continuous activations (e.g., tanh and sigmoid).

Taken together, these two results provide a sharp understanding of generalization in terms of the graph diffusion matrix for graph neural networks. We note that the numerical value of our bounds in their dependence on the graph is much smaller than prior results [16, 38], as is clear from Figure 1a. Moreover, the same trend holds even after taking weight norms into account (see Figure 2, Section 3.3). Further, the Hessian-based bounds (see Lemma 4.3, Section 4) are non-vacuous, matching the scale of empirically observed generalization gaps in Figure 1b.

Finally, motivated by the above analysis, we also present an algorithm that performs gradient updates on perturbed weight matrices of a graph neural network. The key insight is that minimizing the average loss of multiple perturbed models with independent noise injections is equivalent to regularizing f ’s Hessian in expectation. We conduct experiments on several graph classification tasks with Molecular graphs that show the benefit of this algorithm in the fine-tuning setting.

2 Related Work

Generalization Bounds: An article by Zhang et al. (2017) finds that deep nets have enough parameters to memorize real images with random labels, yet they still generalize well if trained with true labels. This article highlights the overparametrized nature of modern deep nets (see also a recent article by Arora [1]), motivating the need for complexity measures beyond classical notions. In the case of two-layer ReLU networks, Neyshabur et al. (2019) show that (path) norm bounds better capture the “effective number of parameters” than VC dimension—which is the number of parameters for piecewise linear activations [5].

For multilayer networks, subsequent works have developed norm, and margin bounds, either via Rademacher complexities [4, 20, 39], or PAC-Bayesian bounds [2, 43, 37, 34]. All of these bounds apply to the fine-tuning setting following the distance from the initialization perspective. Our analysis approach builds on the work of Arora et al. (2018) and Ju et al. (2022). The latter work connects perturbed losses and Hessians for feedforward neural networks, with one limitation Hessians do not show any explicit dependence on the data. This is a critical issue for GNN as we need to incorporate the graph structure in the generalization bound. Our result instead shows an explicit dependence on the graph and applies to message-passing layers that involve additional nonlinear mappings. We will compare our analysis approach and prior analysis in more detail when we present the proofs in Section 4 (see Remark 4.4).

Graph Representation Learning: Most contemporary studies of learning on graphs consider either node-level or graph-level prediction tasks. Our result applies to graph prediction while permitting an extension to node prediction: see Remark 4.2 in Section 4. Most graph neural networks follow an information diffusion mechanism on graphs [46]. Early work takes inspiration

from ConvNets and designs local convolution on graphs, e.g., spectral networks [6], GCN [36], and GraphSAGE [24] (among others). Subsequent works have designed new architectures with graph attention [49] and isomorphism testing [55]. Gilmer et al. (2017) synthesize several models into a framework called message-passing neural networks. Besides, one could also leverage graph structure in the pooling layer (e.g., differentiable pooling and hierarchical pooling [60, 63]). It is conceivable that one can incorporate the model complexity of these approaches into our analysis. Recent work applies pretraining to large-scale graph datasets for learning graph representations [27]. Despite being an effective transfer learning approach, few works have examined the generalization of graph neural nets in the fine-tuning step.

Besides learning on graphs, GNNs are also used for combinatorial optimization [48] and causal reasoning [56]. There is another approach for graph prediction using graph kernels [51] such as the graph neural tangent kernel [11]. Lastly, we remark that graph diffusion processes have been studied in earlier literature on social and information networks [18, 19, 62]. For further references about different applications of GNN, see review articles [23, 7, 13, 54].

Generalization in Graph Neural Networks: Recent work explores generalization by formalizing the role of the algorithm and the alignment between networks and tasks [57]. Esser et al. [14] finds that transductive Rademacher complexity-based bound provides insights into the behavior of GNNs in the stochastic block model. Besides, there are works about size generalization, which refer to performance degradation when models extrapolate to graphs of different sizes from the input [48, 59]. It is conceivable that the new tools we have developed may be useful for studying extrapolation.

Expressivity of Graph Neural Networks: The expressivity of GNN for graph classification can be related to graph isomorphism tests and has connections to one-dimensional Weisfeiler-Lehman testing of graph isomorphism [42, 55]. This implies limitations of GNN for expressing tasks such as counting cycles [45, 8, 3]. The expressiveness view seems orthogonal to generalization, which instead concerns the sample efficiency of learning. For further discussions and references, see a recent survey by Jegelka [30].

3 Sharp Generalization Bounds for Graph Neural Networks

We first introduce the problem setup for analyzing graph neural networks. Then, we state our generalization bounds for graph neural networks and compare them with the prior art. Lastly, we construct an example to argue that our bounds are tight.

3.1 Problem setup

Consider a graph-level prediction task. Suppose we have N examples in the training set; each example is an independent sample from a distribution denoted as \mathcal{D} , which is jointly supported on the feature space \mathcal{X} times the label space \mathcal{Y} . In each example, we have an undirected graph denoted as $G = (V, E)$, which describes the connection between n entities, represented by nodes in V . For example, a node could represent a molecule, and an edge between two nodes is a bond between two molecules. Each node also has a list of d features. Denote all node features as an n by d matrix X . For graph-level prediction tasks, the goal is to predict a graph label y for every example. We will describe a few examples of such tasks later in Section 5.2.

Message-passing neural networks (MPNN). We study a model based on several prior works for graph-level prediction tasks [9, 17, 16, 38]. Let l be the number of layers: the first $l - 1$ layers are diffusion layers, and the last layer is a pooling layer. Let d_t denote the width of each layer for t from

1 up to l . There are several nonlinear mappings in layer t , denoted as ϕ_t , ρ_t , and ψ_t ; further, they are all centered at zero. There is a weight matrix $W^{(t)}$ of dimension d_{t-1} by d_t for transforming neighboring features, and another weight matrix $U^{(t)}$ of dimension d by d_t for transforming the anchor node feature.

For the first $l-1$ layers, we recursively compute the node embedding from the input features $H^{(0)} = X$:

$$H^{(t)} = \phi_t \left(XU^{(t)} + \rho_t(P_G \psi_t(H^{(t-1)}))W^{(t)} \right), \text{ for } t = 1, 2, \dots, l. \quad (1)$$

For the last layer l , we aggregate the embedding of all nodes: let $\mathbf{1}_n$ be a vector with n values of one:

$$H^{(l)} = \frac{1}{n} \mathbf{1}_n^\top H^{(l-1)} W^{(l)}. \quad (2)$$

Note that this setting subsumes many existing GNNs. Several common designs for the graph diffusion matrix P_G would be the adjacency matrix of the graph (denoted as A). P_G can also be the normalized adjacency matrix, $D^{-1}A$, with D being the degree-diagonal matrix. Adding an identity matrix in A is equivalent to adding self-loops in G . For GCN, we set $U^{(t)}$ as zero, ρ_t and ψ_t as identity mappings.

Notations. For any matrix X , let $\|X\|$ denote the largest singular value (or spectral norm) of X . Let $\|X\|_F$ denote the Frobenius norm of X . We use the notation $f(N) \lesssim g(N)$ to indicate that there exists a fixed constant c that does not grow with N such that $f(N) \leq c \cdot g(N)$ for large enough values of N . Let \mathbf{W} and \mathbf{U} denote the union of the W and U matrices in a model f , respectively.

3.2 Main results

Given a message-passing neural network denoted as f , what can we say about its generalization performance, i.e., the gap between population and empirical risks? Let $f(X, G)$ denote the output of f , given input with graph G , node feature matrix X , and label y . The loss of f for this input example is denoted as $\ell(f(X, G), y)$. Let $\hat{L}(f)$ denote the empirical loss of f over the training set. Let $L(f)$ denote the expected loss of f over a random drawn of \mathcal{D} . We are interested in the generalization gap of f , i.e., $L(f) - \hat{L}(f)$. How would the graph diffusion matrix P_G affect the generalization gap of graph neural networks?

To motivate our result, we examine the effect of incorporating graph diffusion in a one-layer linear neural network. That is, we consider $f(X, G)$ to be $\frac{1}{n} \mathbf{1}_n^\top P_G X W^{(1)}$, which does not involve any nonlinear mapping for simplicity of our discussion. In this case, by standard spectral norm inequalities for matrices, the Euclidean norm of f (which is a vector) satisfies:

$$\begin{aligned} \|f(X, G)\| &= \left\| \frac{1}{n} \mathbf{1}_n^\top P_G X W^{(1)} \right\| \\ &\leq \left\| \frac{1}{n} \mathbf{1}_n^\top \right\| \cdot \|P_G\| \cdot \|X\| \cdot \|W^{(1)}\| \end{aligned} \quad (3)$$

Thus, provided that the loss function $\ell(\cdot, y)$ is Lipschitz-continuous, standard arguments imply that the generalization gap of f scales with the spectral norm of P_G (divided by \sqrt{N}) [41]. Let us compare this statement with a fully-connected neural net that averages the node features, i.e., the graph diffusion matrix P_G is the identity matrix. The spectral norm of P_G becomes one. Together, we conclude that the graph structure affects the generalization bound of a single layer GNN by adding the spectral norm of P_G .

Our main result is that incorporating the spectral norm of the *graph diffusion matrix* P_G^{l-1} is sufficient for any l layer MPNN. We note that the dependence is a power of $l-1$ because there are

Table 1: How does the generalization gap of graph neural networks scale with graph properties? In this work, we show spectrally-normalized bounds on P_G and compare our results with prior results in the following table. We let A denote the adjacency matrix, D be the degree-diagonal matrix of A , and l be the depth of the GNN. Previous generalization bounds scale with the graph’s maximum degree denoted as d . Our result instead scales with the spectral norm of P_G and applies to graph isomorphism networks (GIN) [55] and GraphSAGE with mean aggregation [24].

Graph Dependence	GCN	MPNN	GIN	GraphSAGE-Mean
Garg et al. (2020)	d^{l-1}	d^{l-1}	-	-
Liao et al. (2021)	$d^{\frac{l-1}{2}}$	d^{l-1}	-	-
Ours (Theorems 3.1 and 4.5)	1	$\ A\ ^{l-1}$	$\sum_{i=1}^{l-1} \frac{\ A\ ^i}{l-1}$	$\ D^{-1}A\ ^{l-1}$

$l - 1$ graph diffusion layers: see equation (1). Let f be an l -layer network whose weights \mathbf{W}, \mathbf{U} are defined within a hypothesis set \mathcal{H} : For every layer i from 1 up to l , we have that

$$\begin{aligned} \|W^{(i)}\| &\leq s_i, \quad \|W^{(i)}\|_F \leq s_i r_i, \\ \|U^{(i)}\| &\leq s_i, \quad \|U^{(i)}\|_F \leq s_i r_i, \end{aligned} \quad (4)$$

where s_1, s_2, \dots, s_l and r_1, r_2, \dots, r_l are bounds on the spectral norm and stable rank and are all greater than or equal to one, without loss of generality. We now present the full statement.

Theorem 3.1. *Suppose all of the nonlinear activations in $\{\phi_t, \rho_t, \psi_t : \forall t\}$ and the loss function $\ell(\cdot, y)$ (for any fixed label $y \in \mathcal{Y}$) are twice-differentiable, Lipschitz-continuous and their first-order and second-order derivatives are both Lipschitz-continuous.*

With probability at least $1 - \delta$ over the randomness of N independent samples from \mathcal{D} , for any $\delta > 0$, and any $\epsilon > 0$ close to zero, any model f with weight matrices in the set \mathcal{H} satisfies:

$$L(f) \leq (1 + \epsilon) \hat{L}(f) + \sum_{i=1}^l \sqrt{\frac{CBd_i \left(\max_{(X, G, y) \sim \mathcal{D}} \|X\|^2 \|P_G\|^{2(l-1)} \right) \left(r_i^2 \prod_{j=1}^l s_j^2 \right)}{N}} + O\left(\frac{\log(\delta^{-1})}{N^{3/4}}\right), \quad (5)$$

where B is an upper bound on the value of the loss function $\ell(x, y)$ for any $(x, y) \sim \mathcal{D}$, C is a fixed constant depending on the activation, and the loss function (see Eq. (44), Appendix A.2.4).

As a remark, prior works by Garg et al. [16] and Liao et al. [38] consider an MPNN with $W^{(t)}$ and $U^{(t)}$ being the same for t from 1 up to l , motivated by practical designs [17, 33]. Thus, their analysis is conducted separately for GCN and MPNN with weight tying. By contrast, our result allows $W^{(t)}$ and $U^{(t)}$ to be arbitrarily different across different layers. This unifies GCN and MPNN without weight tying in the same framework so that we can unify their analysis. We defer the proof sketch of our result and a discussion to Section 4.

3.3 Comparison with prior art

In Table 1, we compare our result with prior results. We first illustrate the effects of graph properties on the generalization bounds. Then we will also show a numerical comparison to incorporate the other components of the bounds.

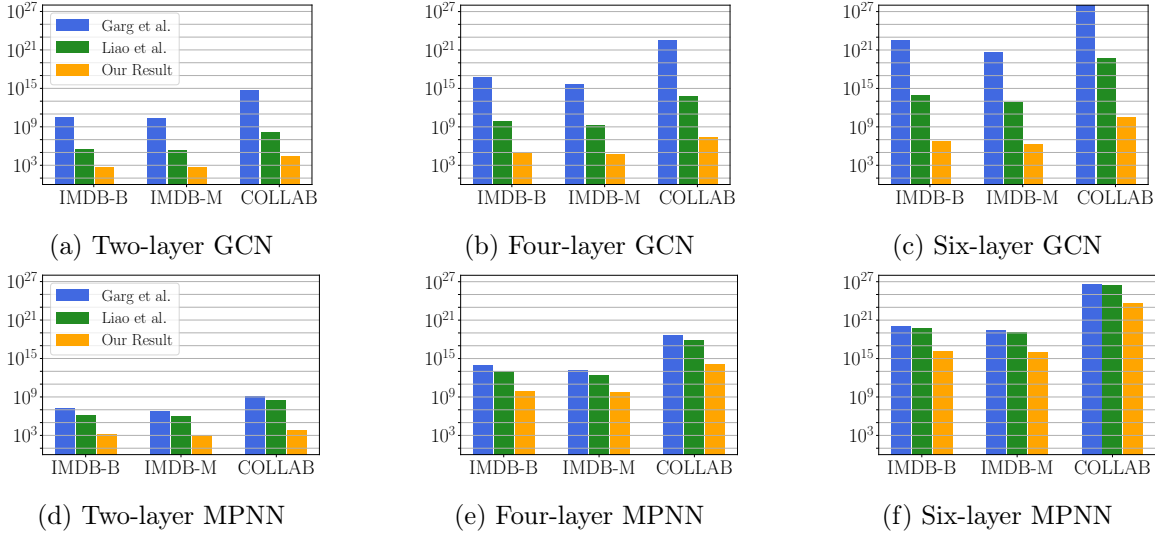


Figure 2: Comparing our result and prior results [16, 38] on three graph classification tasks conducted on GCNs and MPNNs, respectively.

- Suppose P_G is the adjacency matrix of G . Then, one can show that for any undirected graph G , the spectral norm of P_G is less than the maximum degree d (cf. Fact A.1, Appendix A for a proof). This explains why our result is strictly less than prior results for MPNN in Table 1.
- Suppose P_G is the normalized and symmetric adjacency matrix of G : $P_G = \tilde{D}^{-1/2} \tilde{A} \tilde{D}^{-1/2}$, where \tilde{A} is $A + \text{Id}$ and \tilde{D} is the degree-diagonal matrix of \tilde{A} . Then, the spectral norm of P_G is at most one (cf. Fact A.1, Appendix A for a proof). This fact explains why the graph dependence of our result for GCN is 1 in Table 1. Thus, we can see that this provides an exponential improvement compared to the prior results.

Thus, for the above diffusion matrices, we conclude that the spectral norm of P_G is strictly smaller than the maximum degree of graph G (across all graphs in the distribution \mathcal{D}).

Next, we conduct an empirical analysis to compare our results and prior results numerically. Following the setting of prior works, we use two types of models that share their weight matrices across different layers, including GCN [36] and the MPNN specified in Liao et al. [38]. For both models, we evaluate the generalization bounds by varying the network depth l between 2, 4, and 6.

We consider graph prediction tasks on three collaboration networks, including IMDB-B, IMDB-M, and COLLAB [58]. IMDB-B includes a collection of movie collaboration graphs. In each graph, a node represents an actor or an actress, and an edge denotes a collaboration in the same movie. The task is to classify each graph into the movie genre as Action or Romance. The IMDB-M is a multi-class extension with the movie graph label Comedy, Romance, or Sci-Fi. COLLAB includes a list of ego-networks of scientific researchers. Each graph includes a researcher and her collaborators as nodes. An edge in the graph indicates a collaboration between two researchers. The task is to classify each ego-network into the field of the researcher, including High Energy, Condensed Matter, and Astro Physics.

We report the numerical comparison in Figure 2, averaged over three random seeds. Our results are consistently smaller than previous results. As explained in Table 1, the improvement comes from the spectral norm bounds on graphs compared with the max degree bounds.

3.4 A matching lower bound

Next, we show an instance with the same dependence on the graph diffusion matrix as our upper bound. In our example:

- The graph is the complete graph with self-loops inserted in each node. Thus, the adjacency matrix of G is a square matrix with all ones. We will set P_G as the adjacency matrix of G .
- In the first $l - 1$ graph diffusion layers, the activation functions ϕ, ρ, ψ are all linear functions. Further, we fix all the parameters of \mathbf{U} as zero.
- The loss function ℓ is the logistic loss.

Then, we demonstrate a data distribution such that there always exists some weight matrices within \mathcal{H} whose generalization gap must increase in proportion to the spectral norm of P_G^{l-1} and the product of the spectral norm of every layer s_1, s_2, \dots, s_l .

Theorem 3.2. *Let N_0 be a sufficiently large value. For any norms s_1, s_2, \dots, s_n , there exists a data distribution \mathcal{D} on which with probability at least 0.1 over the randomness of N independent samples from \mathcal{D} , for any $N \geq N_0$, the generalization gap of f is greater than the following:*

$$|L(f) - \hat{L}(f)| \gtrsim \sqrt{\frac{\left(\max_{(X, G, y) \sim \mathcal{D}} \|P_G\|^{2(l-1)}\right) \left(\prod_{i=1}^l s_i^2\right)}{N}}. \quad (6)$$

Notice that the lower bound in (6) exhibits the same scaling in terms of $G - \|P_G\|^{l-1}$ —as our upper bound from equation (5). Therefore, we conclude that our spectral norm bound is tight for multilayer MPNN. The proof of the lower bound can be found in Appendix A.3.

Remark 3.3. Our results from Theorem 3.1 and 3.2 together suggest the generalization error bound scales linearly in l . To verify whether this is the case, we conducted an empirical study on three architectures (GCN, GIN-Mean, and GIN-Sum) that measured the growth of generalization errors as the network depth l varies. We find that the generalization error grows sublinearly with l to $\|P_G\|$. We also note that this sublinear growth trend has been captured by our Hessian-based generalization bound (cf. Figure 1a). It would be interesting to understand better why the sublinear trend happens and further provide insight into the behavior of GNN.

Remark 3.4. Theorem 3.2 suggests that in the worst case, the generalization bound would have to scale with the spectral norms of the graph and the weight matrices. Although this is vacuous for large l , later in Lemma 4.1, we show a data-dependent bound using the trace of the Hessians, which is non-vacuous. As shown in Figure 1a, Hessian-based measurements match the scale of actual generalization errors: the green line, calculated based on the trace of the loss Hessian matrix (cf. equation (7)), matches the scale of actual generalization gaps plotted in the yellow line.

4 Proof Techniques and Extensions

Our analysis for dealing with the graph structure seems fundamentally different from the existing analysis. In the margin analysis of Liao et al. [38], the authors also incorporate the graph structure in the perturbation error. For bounding the perturbation error, the authors use a triangle inequality that results in a $(1, \infty)$ norm of the matrix P_G (see Lemma 3.1 of Liao et al. [38] for GCN). We note

that this norm can be larger than the spectral norm by a factor of \sqrt{n} , where n is the number of nodes in G : in the case of a star graph, this norm for the graph diffusion matrix of GCN is \sqrt{n} . By comparison, the spectral norm of the same matrix is less than one (see Fact A.1, Appendix A).

How can we tighten the perturbation error analysis and the dependence on P_G in the generalization bounds, then? Our proof involves two parts:

- **Part I:** By expanding the perturbed loss of a GNN, we prove a bound on the generalization gap using the trace of the Hessian matrix associated with the loss.
- **Part II:** Then, we explicitly bound the trace of the Hessian matrix with the spectral norm of the graph using the Lipschitzness of the activation functions.

Part I: Measuring noise stability using the Hessian. We first state an implicit generalization bound that measures the trace of the Hessian matrix. Let $\mathbf{H}^{(i)}$ denote the Hessian matrix of the loss $\ell(f(X, G), y)$ with respect to layer i 's parameters, for each i from 1 up to l . Particularly, $\mathbf{H}^{(i)}$ is a square matrix whose dimension depends on the number of variables within layer i . Let \mathbf{H} denote the Hessian matrix of the loss $\ell(f(X, G), y)$ over all parameters of f .

Lemma 4.1. *In the setting of Theorem 3.1, with probability at least $1 - \delta$ over the randomness of the N training examples, for any $\delta > 0$ and ϵ close to 0, we get:*

$$L(f) \leq (1 + \epsilon)\hat{L}(f) + (1 + \epsilon) \sum_{i=1}^l \sqrt{\frac{B \cdot \left(\max_{(X, G, y) \sim \mathcal{D}} \text{Tr} [\mathbf{H}^{(i)}[\ell(f(X, G), y)]] \right) s_i^2 r_i^2}{N}} + O\left(\frac{\log(\delta^{-1})}{N^{3/4}}\right). \quad (7)$$

Proof Sketch. At a high level, the above result follows from Taylor's expansion of the perturbed loss. Suppose each parameter of f is perturbed by an independent noise drawn from a Gaussian distribution with mean zero and variance σ^2 . Let $\tilde{\ell}(f(X, G), y)$ be the perturbed loss value of an input example X, G with label y . Let \mathcal{E} denote the noise injections organized in a vector. Using Taylor's expansion of the perturbed loss $\tilde{\ell}$, we get:

$$\tilde{\ell}(f(X, G), y) - \ell(f(X, G), y) = \mathcal{E}^\top \nabla \ell(f(X, G), y) + \frac{1}{2} \mathcal{E}^\top \mathbf{H}[\ell(f(X, G), y)] \mathcal{E} + O(\sigma^3). \quad (8)$$

Notice that the expectation of the first-order expansion term above equals zero. The expectation of the second-order expansion term becomes σ^2 times the trace of the loss Hessian. To derive equation (7), we use a PAC-Bayes bound of McAllester [40, Theorem 2]. There are two parts to this PAC-Bayes bound:

- The expectation of the noise perturbation in equation (8), taken over the injected noise \mathcal{E} ;
- The KL divergence between the prior and the posterior, which is at most $s_i^2 r_i^2$ for layer i , for i from 1 up to l , within the hypothesis set \mathcal{H} .

Thus, one can balance the two parts by adjusting the noise variance at each layer—this leads to the layerwise Hessian decomposition in equation (7).

A critical step is showing the uniform convergence of the Hessian matrix. We achieve this based on the Lipschitz-continuity of the first and twice derivatives of the nonlinear activation mappings. With these conditions, we prove the uniform convergence with a standard ϵ -cover argument. The complete proof can be found in Appendix A.2.1.

Remark 4.2. Our argument in Lemma 4.1 applies to graph-level prediction tasks, which assume an unknown distribution of graphs. A natural question is whether the analysis applies to node-level prediction tasks, which are often treated as semi-supervised learning problems. The issue with directly applying our analysis to semi-supervised learning is that the size of a graph is only finite. Instead, a natural extension would be to think about our graph as a random sample from some population and then argue about generalization in expectation of the random sample. It is conceivable that one can prove a similar spectral norm bound for node prediction in this extension. This would be an interesting question for future work.

Part II: Spectral norm bounds of the trace of the Hessian. Next, we explicitly analyze the trace of the Hessian at each layer. We bound the trace of the Hessian using the spectral norm of the weight matrices and the graph based on the Lipschitz-continuity conditions from Theorem 3.1. Notice that the last layer is a linear pooling layer, which can be deduced from layer $l - 1$. Hence, we consider the first $l - 1$ layers below.

Lemma 4.3. *In the setting of Theorem 3.1, the trace of the loss Hessian matrix $\mathbf{H}^{(i)}$ taken over $W^{(i)}$ and $U^{(i)}$ satisfies the following, for any $i = 1, 2, \dots, l - 1$,*

$$\begin{aligned} & \left| \text{Tr} \left[\mathbf{H}^{(i)} [\ell(f(X, G), y)] \right] \right| \\ & \lesssim s_l^2 \left(\sum_{p=1}^{d_{i-1}} \sum_{q=1}^{d_i} \left\| \frac{\partial^2 H^{(l-1)}}{\partial (W_{p,q}^{(i)})^2} \right\|_F + \sum_{p=1}^{d_0} \sum_{q=1}^{d_i} \left\| \frac{\partial^2 H^{(l-1)}}{\partial (U_{p,q}^{(i)})^2} \right\|_F + \left\| \frac{\partial H^{(l-1)}}{\partial W^{(i)}} \right\|_F^2 + \left\| \frac{\partial H^{(l-1)}}{\partial U^{(i)}} \right\|_F^2 \right) \quad (9) \end{aligned}$$

$$\lesssim \|X\|^2 \|P_G\|^{2(l-1)} \prod_{j=1: j \neq i}^l s_j^2. \quad (10)$$

Proof Sketch. Equation (9) uses the chain rule to expand out the trace of the Hessian and then applies the Lipschitzness of the loss function. Based on this result, equation (10) then bounds the first and second derivatives of $H^{(l-1)}$. This step is achieved via an induction of $\partial H^{(j)}$ and $\partial^2 H^{(j)}$ over $W^{(i)}$ and $U^{(i)}$, for $j = 1, \dots, l - 1$ and $i = 1, \dots, j$. The induction relies on the feedforward architecture and the Lipschitzness of the first and second derivatives. We leave out a few details, such as the constants in equations (9) and (10) that can be found in Appendix A.2.2 and A.2.3. Combining both parts together, we get equation (1).

Remark 4.4. We compare our analysis with the approach of Liao et al. [38]. Both our analysis and Liao et al. [38] follow the PAC-Bayesian framework. But additionally, we explore Lipschitz-continuity properties of the first and second derivatives of the activation functions (e.g., examples of such activations include tanh and sigmoid). This allows us to measure the perturbation loss with Hessians, which captures data-dependent properties much more accurately than the margin analysis of Liao et al. [38]. It would be interesting to understand if one could still achieve spectral norm bounds on graphs under weaker smoothness conditions (see, e.g., Wei and Ma [52]). This is left for future work.

4.1 Extensions

Graph isomorphism networks. This architecture concatenates every layer's embedding together for more expressiveness [55]. A classification layer is used after the layers. Let $V^{(i)}$ denote a d_i by k matrix (recall k is the output dimension). Denote the set of these matrices by \mathcal{V} . We average the loss of all of the classification layers. Let $\hat{L}_{GIN}(f)$ denote the average loss of f over N independent samples of \mathcal{D} . Let $L_{GIN}(f)$ denote the expected loss of f over a random sample of \mathcal{D} . See also equation (45) in Appendix A.4 for their precise definitions.

Next, we state a generalization bound for graph isomorphism networks. Let f be any l -layer MPNN with weights defined in a hypothesis space \mathcal{H} : the parameters of f reside within the constraints from equation (4); further, for every i from 1 up to l , the spectral norm of $V^{(i)}$ is less than s_l . Building on Lemma 4.3, we show a bound that scales with the spectral norm generalization of the averaged graph diffusion matrices. Let P_{GIN} denote the average of $l - 1$ matrices: $P_G, P_G^2, \dots, P_G^{l-1}$. We state the result below.

Corollary 4.5. *Suppose the nonlinear activation mappings and the loss function satisfy the conditions stated in Theorem 3.1. With probability at least $1 - \delta$ for any $\delta \geq 0$, and any ϵ close to zero, any f in \mathcal{H} satisfies:*

$$L_{GIN}(f) \leq (1 + \epsilon)\hat{L}_{GIN}(f) + \sum_{i=1}^l \sqrt{\frac{BCd_i \cdot \left(\max_{(X, G, y) \sim \mathcal{D}} \|X\|^2 \|P_{GIN}\|^2 \right) \left(r_i^2 \prod_{j=1}^l s_j^2 \right)}{N}} + O\left(\frac{\log(\delta^{-1})}{N^{3/4}}\right), \quad (11)$$

where B is an upper bound on the value of the loss function ℓ across the data distribution \mathcal{D} , C is a fixed constant that only depends on the Lipschitz-continuity of the activation mappings and the loss.

The proof can be found in Appendix A.4. In particular, we apply the trace norm bound over the model output of every layer. The classification layer, which only uses a linear transformation, can also be incorporated.

Fine-tuning Graph Neural Networks. We note that all of our bounds can be applied to the fine-tuning setting, where a graph neural network is initialized with pretrained weights and then fine-tuned on the target task. The results can be extended to this setting by setting the norm bounds within equation (4) as the distance between the pretrained and fine-tuned model.

5 An Algorithm for Fine-tuning Graph Neural Networks

A common practice to apply deep networks on graphs is to fit pretrained GNNs, which can be fine-tuned on a target task. Typically, only a small amount of data is available for fine-tuning. Thus, the fine-tuned model may overfit the training data, incurring a large generalization gap. A central insight from our analysis is that maintaining a small perturbed loss ensures lower generalization gaps. Motivated by this observation, we design an algorithm to minimize the perturbed risk of GNN.

Let f denote a GNN and $\tilde{\ell}(f)$ be the perturbed loss of f , with noise injected inside f 's weight matrices. Recall from step (8) that $\tilde{\ell}(f)$ is equal to $\ell(f)$ plus several expansion terms. In particular, minimizing the expectation of $\tilde{\ell}(f)$ is equivalent to minimizing $\hat{L}(f)$ plus the trace of the Hessian matrix. To estimate this expectation, we sample several noise perturbations independently. Because Taylor's expansion of $\tilde{\ell}(f)$ also involves the gradient, we cancel this out by computing the perturbed loss with the negated perturbation. Algorithm 1 describes the complete procedure.

We evaluate the above algorithm for fine-tuning pretrained GNNs. Empirical results reveal that this algorithm achieves better test performance compared with existing regularization methods for five graph classification tasks. The code repository for reproducing the experiments is at <https://github.com/NEU-StatsML-Research/Generalization-in-graph-neural-networks>.

5.1 Experimental setup

We focus on graph classification tasks, including five datasets from the MoleculeNet benchmark [53]. Each dataset aims to predict whether a molecule has a certain chemical property given its graph representation. We use pretrained GINs from Hu et al. [27] and fine-tune the model on each

Algorithm 1 Algorithms for fine-tuning graph neural networks

Input: A training dataset $\{(X_i, G_i, y_i)\}_{i=1}^N$ with node feature X_i , graph G_i , and graph-level label y_i , for $i = 1, \dots, N$.

Require: Number of perturbations m , noise variance σ^2 , learning rate η , and number of epochs T .

Output: A trained model $f^{(T)}$.

- 1: At $t = 0$, initialize the parameters of $f^{(0)}$ with pretrained GNN weight matrices.
- 2: **for** $1 \leq t \leq T$ **do**
- 3: **for** $1 \leq i \leq m$ **do**
- 4: Add perturbation \mathcal{E}_i drawn from a normal distribution with mean zero and variance σ^2 .
- 5: Let $\tilde{L}_i(f^{(t-1)})$ be the training loss of the model $f^{(t-1)}$ with weight matrix perturbed by \mathcal{E}_i .
- 6: Let $\tilde{L}'_i(f^{(t-1)})$ be the training loss of the model $f^{(t-1)}$ with weight matrix perturbed by $-\mathcal{E}_i$.
- 7: **end for**
- 8: Use stochastic gradient descent to update $f^{(t)}$ as $f^{(t-1)} - \frac{\eta}{2m} \sum_{i=1}^m (\nabla \tilde{L}_i(f^{(t-1)}) + \nabla \tilde{L}'_i(f^{(t-1)}))$.
- 9: **end for**

downstream task. Following their experimental setup, we use the scaffold split for the dataset, and the model architecture is fixed for all five datasets. Each model has 5 layers; each layer has 300 hidden units and uses average pooling in the readout layer. We set the parameters, such as the learning rate and the number of epochs following their setup.

We compare our algorithm with previous regularization methods that serve as benchmark approaches for improving generalization. This includes early stopping, weight decay, dropout, weight averaging [29], and distance-based regularization [21]. For implementing our algorithm, we set the number of perturbations as 10 and choose the noise standard deviation σ with a grid search in $\{0.01, 0.02, 0.05, 0.1, 0.2, 0.5\}$.

5.2 Experimental results

Table 2 reports the test ROC-AUC performance averaged over multiple binary prediction tasks in each dataset. Comparing the average ranks of methods across datasets, our algorithm outperforms baselines on all five molecular property prediction datasets. The results support our theoretical analysis that the noise stability property of GNN is a strong measure of empirical generalization performance. Next, we provide details insights from applying our algorithm.

First, we hypothesize that our algorithm is particularly effective when the empirical generalization gap is large. To test the hypothesis, we vary the size of the training set in the BACE dataset; we compare the performance of our algorithm with early stopping until epoch 100. We plot the generalization gap between the training and test losses during training, shown in Figure 3a-3b. As the trend shows, our algorithm consistently reduces the generalization gap, particularly when the training set size N is 600.

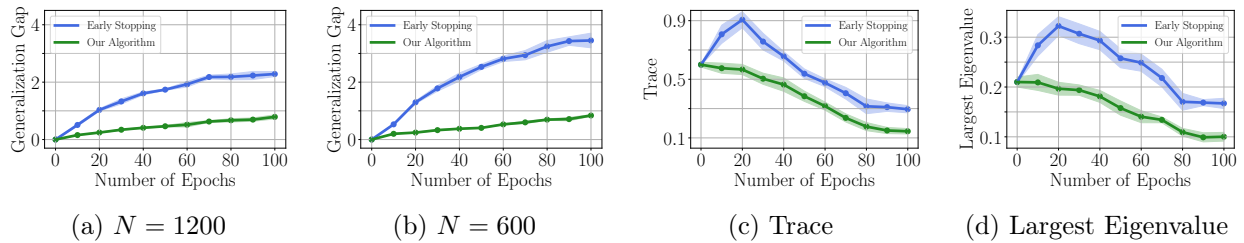
Second, we hypothesize that our algorithm helps reduce the trace of the Hessian matrix (associated with the loss). We validate this by plotting the trace of the Hessian as the number of epochs progresses during training, again using the BACE dataset as an example. Specifically, we average the trace over the training dataset. Figure 3c shows the averaged trace values during the fine-tuning process. The results confirm that noise stability optimization reduces the trace of the Hessian matrix (more significantly than early stopping). We note that noise stability optimization also reduces the largest eigenvalue of the Hessian matrix, along with reducing the trace. This can be seen in Figure 3d.

Lastly, we study the number of perturbations used in our algorithm. While more perturbations would lead to a better estimation of the noisy stability, we observe that using 10 perturbations is sufficient for getting the most gain. We also validate that using negated perturbations consistently

Table 2: Test ROC-AUC (%) score for five molecular property prediction datasets with different regularization methods. The reported results are averaged over five random seeds.

Dataset	SIDER	ClinTox	BACE	BBBP	Tox21
# Molecule Graphs	1,427	1,478	1,513	2,039	7,831
# Binary Prediction Tasks	27	2	1	1	12
Early Stopping	61.06 \pm 1.48	68.25 \pm 2.63	82.86 \pm 0.95	67.80 \pm 1.05	77.52 \pm 0.23
Weight Decay	61.30 \pm 0.21	67.43 \pm 2.88	83.72 \pm 0.99	67.98 \pm 2.41	78.23 \pm 0.35
Dropout	63.90 \pm 0.90	73.70 \pm 2.80	84.50 \pm 0.70	68.07 \pm 1.30	78.30 \pm 0.30
Weight Averaging	63.67 \pm 0.34	78.78 \pm 1.49	83.93 \pm 0.36	70.26 \pm 0.24	77.59 \pm 0.11
Distance-based Reg.	64.36 \pm 0.48	76.68 \pm 1.19	84.65 \pm 0.48	70.37 \pm 0.44	78.62 \pm 0.24
Ours (Alg. 1)	65.13\pm0.18	80.18\pm0.82	85.07\pm0.43	71.22\pm0.36	79.31\pm0.24

Figure 3: In Figures 3a and 3b, we show that our algorithm is particularly effective at reducing the generalization gap for small training dataset sizes N . In Figures 3c and 3d, we find that both the trace and the largest eigenvalue of the loss Hessian matrix decreased during training.



performs better than not using them across five datasets. This is because the negated perturbation cancels out the first-order term in Taylor’s expansion. In our ablation study, we find that adding the negated perturbation performs better than not using it by 1% on average over the five datasets.

Remark 5.1. We note that noise stability optimization is closely related to sharpness-aware minimization (SAM) [15]. Noise stability optimization differs in two aspects compared with SAM. First, SAM requires solving constrained minimax optimization, which may not even be differentiable [10]. Our objective remains the same after perturbation. Second, SAM reduces the largest eigenvalue of the Hessian matrix, which can be seen from Taylor’s expansion of $\tilde{\ell}(f)$. We reduce the trace of the Hessian matrix, which includes reducing the largest eigenvalue as part of the trace. There is another related work that regularizes noise stability in NLP [28]. Their approach adds noise perturbation in the input and regularizes the loss change in the output. Our approach directly adds the perturbation in the weight matrices.

6 Conclusion

This work develops generalization bounds for graph neural networks with a sharp dependence on the graph diffusion matrix. The results are achieved within a unified setting that significantly extends prior works. In particular, we answer an open question mentioned in Liao et al. [38]: a refined PAC-Bayesian analysis can improve the generalization bounds for message-passing neural networks. These bounds are obtained by analyzing the trace of the Hessian matrix with the Lipschitz-continuity of the activation functions. Empirical findings suggest that the Hessian-based bound matches observed gaps on real-world graphs. Thus, our work also develops a practical tool to measure the

generalization performance of graph neural networks. The algorithmic results with noise stability optimization further demonstrate the practical implication of our findings.

Our work opens up many interesting questions for future work. Could the new tools we have developed be used to study generalization in graph attention networks [49]? Could Hessians be used for measuring out-of-distribution generalization gaps of graph neural networks? We remark that in a recent follow-up paper [35], we provide a rigorous analysis of the convergence rates of our algorithm presented in the experiments, showing matching upper and lower bounds given Lipschitz-continuous conditions of the gradients.

Acknowledgement

Thanks to Renjie Liao, Haoyu He, and the anonymous referees for providing constructive feedback on our work. Thanks to Yang Yuan for the helpful discussions. HZ is grateful to Stefanie Jegelka for an invitation to present this paper at her lab meeting. HJ and DL acknowledge financial support from the startup fund of Khoury College of Computer Sciences, Northeastern University.

References

- [1] S. Arora (2021). “Technical perspective: Why don’t today’s deep nets overfit to their training data?” In: *Communications of the ACM*.
- [2] S. Arora, R. Ge, B. Neyshabur, and Y. Zhang (2018). “Stronger generalization bounds for deep nets via a compression approach”. In: *ICML*.
- [3] W. Azizian and M. Lelarge (2021). “Expressive power of invariant and equivariant graph neural networks”. In: *ICLR*.
- [4] P. Bartlett, D. J. Foster, and M. Telgarsky (2017). “Spectrally-normalized margin bounds for neural networks”. In: *NeurIPS*.
- [5] P. Bartlett, N. Harvey, C. Liaw, and A. Mehrabian (2019). “Nearly-tight VC-dimension and pseudodimension bounds for piecewise linear neural networks”. In: *JMLR*.
- [6] J. Bruna, W. Zaremba, A. Szlam, and Y. LeCun (2014). “Spectral networks and locally connected networks on graphs”. In: *ICLR*.
- [7] I. Chami, S. Abu-El-Haija, B. Perozzi, C. Ré, and K. Murphy (2020). “Machine learning on graphs: A model and comprehensive taxonomy”. In: *arXiv preprint arXiv:2005.03675*, p. 1.
- [8] Z. Chen, L. Chen, S. Villar, and J. Bruna (2020). “Can graph neural networks count substructures?” In: *NeurIPS*.
- [9] H. Dai, B. Dai, and L. Song (2016). “Discriminative embeddings of latent variable models for structured data”. In: *ICML*.
- [10] C. Daskalakis, S. Skoulakis, and M. Zampetakis (2021). “The complexity of constrained min-max optimization”. In: *STOC*.
- [11] S. S. Du, K. Hou, R. R. Salakhutdinov, B. Poczos, R. Wang, and K. Xu (2019). “Graph neural tangent kernel: Fusing graph neural networks with graph kernels”. In: *NeurIPS*.
- [12] G. K. Dziugaite and D. M. Roy (2017). “Computing nonvacuous generalization bounds for deep (stochastic) neural networks with many more parameters than training data”. In: *UAI*.
- [13] F. Errica, M. Podda, D. Bacciu, and A. Micheli (2020). “A fair comparison of graph neural networks for graph classification”. In: *ICLR*.
- [14] P. Esser, L. Chennuru Vankadara, and D. Ghoshdastidar (2021). “Learning theory can (sometimes) explain generalisation in graph neural networks”. In: *NeurIPS*.

[15] P. Foret, A. Kleiner, H. Mobahi, and B. Neyshabur (2021). “Sharpness-aware minimization for efficiently improving generalization”. In: *ICLR*.

[16] V. Garg, S. Jegelka, and T. Jaakkola (2020). “Generalization and representational limits of graph neural networks”. In: *ICML*.

[17] J. Gilmer, S. S. Schoenholz, P. F. Riley, O. Vinyals, and G. E. Dahl (2017). “Neural message passing for quantum chemistry”. In: *ICML*.

[18] A. Goel, S. Khanna, S. Raghvendra, and H. Zhang (2014). “Connectivity in random forests and credit networks”. In: *SODA*.

[19] A. Goel, K. Munagala, A. Sharma, and H. Zhang (2015). “A note on modeling retweet cascades on Twitter”. In: *Workshop on Algorithms and Models for the Web-Graph, 2015*.

[20] N. Golowich, A. Rakhlin, and O. Shamir (2018). “Size-independent sample complexity of neural networks”. In: *COLT*.

[21] H. Gouk, T. M. Hospedales, and M. Pontil (2021). “Distance-Based Regularisation of Deep Networks for Fine-Tuning”. In: *ICLR*.

[22] B. Guedj (2019). “A Primer on PAC-Bayesian Learning”. In: *Proceedings of the French Mathematical Society*.

[23] W. Hamilton, R. Ying, and J. Leskovec (2017a). “Representation learning on graphs: Methods and applications”. In: *arXiv preprint arXiv:1709.05584*.

[24] W. Hamilton, Z. Ying, and J. Leskovec (2017b). “Inductive representation learning on large graphs”. In: *NeurIPS*.

[25] M. Hardt and B. Recht (2021). “Patterns, predictions, and actions: A story about machine learning”. In: *arXiv preprint arXiv:2102.05242*.

[26] M. Hardt, B. Recht, and Y. Singer (2016). “Train faster, generalize better: Stability of stochastic gradient descent”. In: *ICML*.

[27] W. Hu, B. Liu, J. Gomes, M. Zitnik, P. Liang, V. Pande, and J. Leskovec (2020). “Strategies for pre-training graph neural networks”. In: *ICLR*.

[28] H. Hua, X. Li, D. Dou, C.-Z. Xu, and J. Luo (2021). “Noise stability regularization for improving BERT fine-tuning”. In: *ACL*.

[29] P. Izmailov, D. Podoprikhin, T. Garipov, D. Vetrov, and A. G. Wilson (2018). “Averaging weights leads to wider optima and better generalization”. In: *UAI*.

[30] S. Jegelka (2022). “Theory of Graph Neural Networks: Representation and Learning”. In: *arXiv preprint arXiv:2204.07697*.

[31] Y. Jiang, B. Neyshabur, H. Mobahi, D. Krishnan, and S. Bengio (2020). “Fantastic generalization measures and where to find them”. In: *ICLR*.

[32] C. Jin, P. Netrapalli, R. Ge, S. M. Kakade, and M. I. Jordan (2019). “A short note on concentration inequalities for random vectors with subgaussian norm”. In: *arXiv preprint arXiv:1902.03736*.

[33] W. Jin, R. Barzilay, and T. Jaakkola (2018). “Junction tree variational autoencoder for molecular graph generation”. In: *ICML*.

[34] H. Ju, D. Li, and H. R. Zhang (2022). “Robust Fine-Tuning of Deep Neural Networks with Hessian-based Generalization Guarantees”. In: *ICML*.

[35] — (2023). “Noise Stability Optimization for Flat Minima with Optimal Convergence Rates”. In: *arXiv preprint arXiv:2306.08553*.

[36] T. N. Kipf and M. Welling (2017). “Semi-supervised classification with graph convolutional networks”. In: *ICLR*.

[37] D. Li and H. R. Zhang (2021). “Improved regularization and robustness for fine-tuning in neural networks”. In: *NeurIPS*.

[38] R. Liao, R. Urtasun, and R. Zemel (2021). “A PAC-Bayesian Approach to Generalization Bounds for Graph Neural Networks”. In: *ICLR*.

[39] P. M. Long and H. Sedghi (2020). “Generalization bounds for deep convolutional neural networks”. In: *ICLR*.

[40] D. McAllester (2013). “A PAC-Bayesian tutorial with a dropout bound”. In: *arXiv preprint arXiv:1307.2118*.

[41] M. Mohri, A. Rostamizadeh, and A. Talwalkar (2018). *Foundations of machine learning*. MIT press.

[42] C. Morris, M. Ritzert, M. Fey, W. L. Hamilton, J. E. Lenssen, G. Rattan, and M. Grohe (2019). “Weisfeiler and leman go neural: Higher-order graph neural networks”. In: *AAAI*.

[43] B. Neyshabur, S. Bhojanapalli, and N. Srebro (2018). “A pac-bayesian approach to spectrally-normalized margin bounds for neural networks”. In: *ICLR*.

[44] B. Neyshabur, Z. Li, S. Bhojanapalli, Y. LeCun, and N. Srebro (2019). “Towards understanding the role of over-parametrization in generalization of neural networks”. In: *ICLR*.

[45] R. Sato, M. Yamada, and H. Kashima (2019). “Approximation ratios of graph neural networks for combinatorial problems”. In: *NeurIPS*.

[46] F. Scarselli, M. Gori, A. C. Tsoi, M. Hagenbuchner, and G. Monfardini (2008). “The graph neural network model”. In: *IEEE transactions on neural networks*.

[47] F. Scarselli, A. C. Tsoi, and M. Hagenbuchner (2018). “The vapnik–chervonenkis dimension of graph and recursive neural networks”. In: *Neural Networks*.

[48] D. Selsam, M. Lamm, B. Bünz, P. Liang, L. de Moura, and D. L. Dill (2019). “Learning a SAT solver from single-bit supervision”. In: *ICLR*.

[49] P. Veličković, G. Cucurull, A. Casanova, A. Romero, P. Lio, and Y. Bengio (2018). “Graph attention networks”. In: *ICLR*.

[50] S. Verma and Z.-L. Zhang (2019). “Stability and generalization of graph convolutional neural networks”. In: *KDD*.

[51] S. Vishwanathan, N. Schraudolph, R. Kondor, and K. Borgwardt (2010). “Graph kernels”. In: *JMLR*.

[52] C. Wei and T. Ma (2020). “Data-dependent sample complexity of deep neural networks via lipschitz augmentation”. In: *NeurIPS*.

[53] Z. Wu, B. Ramsundar, E. N. Feinberg, J. Gomes, C. Geniesse, A. S. Pappu, K. Leswing, and V. Pande (2018). “MoleculeNet: a benchmark for molecular machine learning”. In: *Chemical science*.

[54] Z. Wu, S. Pan, F. Chen, G. Long, C. Zhang, and Y. Philip (2020). “A comprehensive survey on graph neural networks”. In: *IEEE transactions on neural networks and learning systems*.

[55] K. Xu, W. Hu, J. Leskovec, and S. Jegelka (2019). “How powerful are graph neural networks?” In: *ICLR*.

[56] K. Xu, J. Li, M. Zhang, S. S. Du, K.-i. Kawarabayashi, and S. Jegelka (2020). “What can neural networks reason about?” In: *ICLR*.

[57] K. Xu, M. Zhang, J. Li, S. S. Du, K.-i. Kawarabayashi, and S. Jegelka (2021). “How neural networks extrapolate: From feedforward to graph neural networks”. In: *ICLR*.

[58] P. Yanardag and S. Vishwanathan (2015). “Deep graph kernels”. In: *KDD*.

[59] G. Yehudai, E. Fetaya, E. Meirom, G. Chechik, and H. Maron (2021). “From local structures to size generalization in graph neural networks”. In: *ICML*.

[60] Z. Ying, J. You, C. Morris, X. Ren, W. Hamilton, and J. Leskovec (2018). “Hierarchical graph representation learning with differentiable pooling”. In: *NeurIPS*.

[61] C. Zhang, S. Bengio, M. Hardt, B. Recht, and O. Vinyals (2017). “Understanding deep learning requires rethinking generalization”. In: *ICLR*.

- [62] H. Zhang, H. Yu, and A. Goel (2019). “Pruning based distance sketches with provable guarantees on random graphs”. In: *WWW*.
- [63] M. Zhang, Z. Cui, M. Neumann, and Y. Chen (2018). “An end-to-end deep learning architecture for graph classification”. In: *AAAI*.

Organization. In Appendix A, we state the complete proofs for our results. In Appendix B, we describe extra experiment details to complement our results.

A Proofs

This section provides the complete proofs for our results in Section 3. First, we state several notations and facts needed in the proofs. Then we provide the proof of the Hessian-based generalization bound for MPNN, as stated in Lemma 4.1. After that, in Appendix A.2, we provide the proof of Theorem 3.1, a key step of which is the proof of Lemma 4.3. Next, in Appendix A.3, we state the proof of the lower bound. Lastly, in Appendix A.4, we will provide proof for the case of graph isomorphism networks.

First, we state several facts about graphs and provide a short proof of them.

Fact A.1. *Let $G = (V, E)$ be an undirected graph. Let d_G be the maximum degree of G .*

- a) *Let A be the adjacency matrix of G . Then, the adjacency matrix satisfies: $\sqrt{d_G} \leq \|A\| \leq d_G$.*
- b) *The symmetric and degree-normalized adjacency matrix satisfies $\|D^{-1/2}AD^{-1/2}\| \leq 1$.*

Proof. Based on the definition of the spectral norm, we get

$$\|A\| = \max_{\|x\|=1} x^\top Ax = \max_{\|x\|=1} \sum_{(i,j) \in E} x_i x_j \leq \max_{\|x\|=1} \sum_{(i,j) \in E} \frac{1}{2}(x_i^2 + x_j^2) \leq d_G \sum_{i \in V} x_i^2 = d_G.$$

Assume that node i has the maximum degree d_G . Denote edges set $E_i = \{(i, i_k)\}_{k=1}^{d_G} \subseteq E$. Let $x_i = \frac{1}{\sqrt{2}}$, $x_{i_k} = \frac{1}{\sqrt{2d_G}}$ for all $k = 1, \dots, d_G$. The rest entries of x are equal to zero. Thus, x is a normalized vector. Next, we have

$$\|A\| = \max_{\|x\|=1} \sum_{(i,j) \in E} x_i x_j \geq \max_{\|x\|=1} 2 \sum_{(i,j) \in E_i} x_i x_j = 2d_G \cdot \frac{1}{\sqrt{2}} \frac{1}{\sqrt{2d_G}} = \sqrt{d_G}.$$

An example in which $\|P_G\|$ gets close to $\sqrt{d_G}$ is the star graph. An example in which $\|P_G\|$ gets close to d_G is the complete graph.

Next, we focus on case b). From the definition of the spectral norm, we know

$$\begin{aligned} \|D^{-1/2}AD^{-1/2}\| &= \max_{\|x\|=1} x^\top (D^{-1/2}AD^{-1/2})x = \max_{\|x\|=1} \sum_{(i,j) \in E} \frac{x_i x_j}{\sqrt{d_i d_j}} \\ &\leq \max_{\|x\|=1} \sum_{(i,j) \in E} \frac{x_i^2}{2d_i} + \frac{x_j^2}{2d_j} = \sum_{i \in V} x_i^2 = 1. \end{aligned}$$

During the middle of the above step, we used the Cauchy-Schwartz inequality. The proof of this result is now completed.

Notations: For two matrices X and Y that are both of dimension d_1 by d_2 , the Hadamard product of X and Y , denoted as $X \odot Y$, is equal to the entrywise product of X and Y .

A.1 Proof of our PAC-Bayesian bound (Lemma 4.1)

To be precise, we will restate the conditions required in Theorem 3.1 separately below. The conditions are exactly the same as stated in Section 3.

Assumption A.2. *Assume that all the activation functions $\phi_i(\cdot), \rho_i(\cdot), \psi_i(\cdot)$ for any $1 \leq i \leq l-1$ and the loss function $\ell(x, y)$ over x are twice-differentiable and κ_0 -Lipschitz. Their first-order derivatives are κ_1 -Lipschitz and their second-order derivatives are κ_2 -Lipschitz.*

Based on the above assumption, we provide the precise statement for Taylor's expansion, used in equation (8).

Proposition A.3. *In the setting of Theorem 3.1, suppose each parameter in layer i is perturbed by an independent noise drawn from $\mathcal{N}(0, \sigma_i^2)$. Let $\tilde{\ell}(f(X, G), y)$ be the perturbed loss function with noise perturbation injection vector \mathcal{E} on all parameters \mathbf{W} and \mathbf{U} . There exist some fixed value C_1 that do not grow with N and $1/\delta$ such that*

$$\left| \tilde{\ell}(f(X, G), y) - \ell(f(X, G), y) - \frac{1}{2} \sum_{i=1}^l \sigma_i^2 \text{Tr} \left[\mathbf{H}^{(i)} [\ell(f(X, G), y)] \right] \right| \leq C_1 \sum_{i=1}^l \sigma_i^3.$$

Proof. By Taylor's expansion, the following identity holds

$$\tilde{\ell}(f(X, G), y) - \ell(f(X, G), y) = \mathbb{E}_{\mathcal{E}} \left[\mathcal{E}^\top \nabla \ell(f) + \frac{1}{2} \mathcal{E}^\top \mathbf{H}[\ell(f)] \mathcal{E} + R(\ell(f), \mathcal{E}) \right].$$

where $R(\ell(f), \mathcal{E})$ is the rest of the first order and the second order terms. Since each entry in \mathcal{E} follows the normal distribution, we have $\mathbb{E}_{\mathcal{E}} [\mathcal{E}^\top \nabla \ell(f)] = 0$. The Hessian term turns to

$$\mathcal{E}^\top \mathbf{H}[\ell(f)] \mathcal{E} = \sum_{i=1}^l \sigma_i^2 \text{Tr} \left[\mathbf{H}^{(i)} [\ell(f(X, G), y)] \right].$$

Since the readout layer is linear, by Proposition A.4, there exists a fixed constant \bar{C} that does not grow with N and δ^{-1} such that $|R(\ell(f), \mathcal{E})| \leq \bar{C} \|\mathcal{E}\|^3$. Based on Jin et al. [32, Lemma 2], for any x drawn from a normal distribution $\mathcal{N}(0, \sigma^2)$, we have $\mathbb{E}[x^3] \leq 6\sigma^3$. Hence, we get $\mathbb{E}[R(\ell(f), \mathcal{E})] \leq C_1 \sum_{i=1}^l \sigma_i^3$, where $C_1 = O(h^2 \bar{C})$ is a fixed constant. Thus, we have finished the proof.

Next, we state a Lipschitz-continuity upper bound of the network output at each layer. This will be needed in the ϵ -covering argument later in the proof of Theorem 3.1. To simplify the notation, we will abbreviate explicit constants that do not grow with N and $1/\delta$ in the notation \lesssim ; more specifically, we use $A(n) \lesssim B(n)$ to indicate that there exists a function c that does not depend on N and $1/\delta$ such that $A(n) \leq c \cdot B(n)$ for large enough values of n .

Proposition A.4. *In the setting of Theorem 3.1, for any $j = 1, \dots, l-1$, the change in the Hessian of output of the j layer network $H^{(j)}$ with respect to W_i and U_i under perturbation on W and U can be bounded as follows:*

$$\left\| \mathbf{H}_W^{(i)} [\tilde{H}^{(j)}] - \mathbf{H}_W^{(i)} [H^{(j)}] \right\|_F \lesssim \sum_{t=1}^j \left(\|\Delta U^{(t)}\| + \|\Delta W^{(t)}\| \right). \quad (12)$$

$$\left\| \mathbf{H}_U^{(i)} [\tilde{H}^{(j)}] - \mathbf{H}_U^{(i)} [H^{(j)}] \right\|_F \lesssim \sum_{t=1}^j \left(\|\Delta U^{(t)}\| + \|\Delta W^{(t)}\| \right). \quad (13)$$

Above, the notation $\mathbf{H}_{\mathbf{W}}^{(i)}[\tilde{H}^{(j)}]$ is the perturbation of the Hessian matrix of $H^{(j)}$ by $\Delta\mathbf{W}$ and $\Delta\mathbf{U}$, specific to the variables of \mathbf{W} ; likewise, $\mathbf{H}_{\mathbf{U}}^{(i)}[\tilde{H}^{(j)}]$ is the perturbation of the Hessian matrix specific to the variables of \mathbf{U} .

The proof of Proposition A.4 will be deferred until Appendix A.1.1. Based on Propositions A.3 and A.4, now we are ready to present the proof of Lemma 4.1.

Proof of Lemma 4.1. First, we separate the gap of $L(f)$ and $\frac{1}{\beta}\hat{L}(f)$ into three parts:

$$L(f) - \frac{1}{\beta}\hat{L}(f) = \underbrace{\mathbb{E}_{(X,G,y) \sim \mathcal{D}} [\ell(f(X, G), y)] - \mathbb{E}_{(X,G,y) \sim \mathcal{D}} [\tilde{\ell}(f(X, G), y)]}_{E_1} + \underbrace{\mathbb{E}_{(X,G,y) \sim \mathcal{D}} [\tilde{\ell}(f(X, G), y)]}_{E_2} - \frac{1}{\beta} \left(\frac{1}{N} \sum_{i=1}^N \tilde{\ell}(f(X_i, G_i), y_i) \right) + \underbrace{\frac{1}{\beta} \left(\frac{1}{N} \sum_{i=1}^N \tilde{\ell}(f(X_i, G_i), y_i) \right) - \frac{1}{\beta} \left(\frac{1}{N} \sum_{i=1}^N \ell(f(X_i, G_i), y_i) \right)}_{E_2}.$$

for any $\beta \in (0, 1)$. Above, $\tilde{\ell}(f(X, G), y)$ is the perturbed loss from $\ell(f(X, G), y)$ with noise injections \mathcal{E} added to all the parameters in \mathbf{W} and \mathbf{U} . By Taylor's expansion from Proposition A.3, we can bound the difference between $\tilde{\ell}(f(X, G), y)$ and $\ell(f(X, G), y)$ with the trace of the Hessian. Therefore

$$\begin{aligned} L(f) - \frac{1}{\beta}\hat{L}(f) &\leq - \mathbb{E}_{(X,G,y) \sim \mathcal{D}} \left[\frac{1}{2} \sum_{i=1}^l \sigma_i^2 \text{Tr} [\mathbf{H}^{(i)}[\ell(f(X, G), y)]] \right] + \sum_{i=1}^l C_1 \sigma_i^3 \\ &\quad \text{(by Prop. A.3 for } E_1\text{)} \\ &\quad + \left(\mathbb{E}_{(X,G,y) \sim \mathcal{D}} [\tilde{\ell}(f(X, G), y)] - \frac{1}{\beta} \left(\frac{1}{N} \sum_{i=1}^N \tilde{\ell}(f(X_i, G_i), y_i) \right) \right) \\ &\quad + \frac{1}{2\beta} \sum_{i=1}^l \sigma_i^2 \left(\frac{1}{N} \sum_{j=1}^N \text{Tr} [\mathbf{H}^{(i)}[\ell(f(X_j, G_j), y_j)]] \right) + \frac{1}{\beta} \sum_{i=1}^l C_1 \sigma_i^3. \\ &\quad \text{(by Prop. A.3 for } E_2\text{)} \end{aligned}$$

By rearranging the above equation, we get the following:

$$\begin{aligned} L(f) - \frac{1}{\beta}\hat{L}(f) &\leq \frac{1}{2} \sum_{i=1}^l \sigma_i^2 \left(\underbrace{\frac{1}{N} \sum_{j=1}^N \text{Tr} [\mathbf{H}^{(i)}[\ell(f(X_j, G_j), y_j)]]}_{E_3} - \mathbb{E}_{(X,G,y) \sim \mathcal{D}} [\text{Tr} [\mathbf{H}^{(i)}[\ell(f(X, G), y)]]] \right) \\ &\quad + \frac{1}{2} \left(\frac{1}{\beta} - 1 \right) \underbrace{\sum_{i=1}^l \frac{\sigma_i^2}{N} \sum_{j=1}^N \text{Tr} [\mathbf{H}^{(i)}[\ell(f(X_j, G_j), y_j)]]}_{E_4} \\ &\quad + \left(1 + \frac{1}{\beta} \right) C_1 \sum_{i=1}^l \sigma_i^3 + \underbrace{\mathbb{E}_{(X,G,y) \sim \mathcal{D}} [\tilde{\ell}(f(X, G), y)] - \frac{1}{\beta N} \sum_{i=1}^N \tilde{\ell}(f(X_i, G_i), y_i)}_{E_5}. \end{aligned}$$

Based on Proposition A.4, the Hessian operator $\mathbf{H}^{(i)}$ is Lipschitz-continuous for some parameter that does not depend on N and $1/\delta$, for any $i = 1, 2, \dots, l$. Therefore, from Ju et al. [34, Lemma 2.4], there exist some fixed values C_2, C_3 that do not grow with N and $1/\delta$, such that with probability at

least $1 - \delta$ over the randomness of the training set. Therefore, the matrix inside the trace of E_3 satisfies

$$\left\| \frac{1}{N} \sum_{j=1}^N \mathbf{H}^{(i)}[\ell(f(X_j, G_j), y_j)] - \mathbb{E}_{(X, G, y) \sim \mathcal{D}} \left[\mathbf{H}^{(i)}[\ell(f(X, G), y)] \right] \right\|_F \leq \frac{C_2 \sqrt{\log(C_3 N / \delta)}}{\sqrt{N}}, \quad (14)$$

for any $i = 1, \dots, l$. Thus, by the Cauchy-Schwartz inequality, E_3 is less than $\sqrt{2h^2}$ times the RHS of equation (14). Suppose the loss function $\ell(f(X, G), y)$ lies in a bounded range $[0, B]$ given any $(X, G, y) \sim \mathcal{D}$. By the PAC-Bayes bound of McAllester [40, Theorem 2] (see also Guedj [22]), we choose \mathbf{U} as a prior distribution and $\mathbf{W} + \mathbf{U}$ as a posterior distribution. For any $\beta \in (0, 1)$ and $\delta \in [0, 1]$, with probability at least $1 - \delta$, E_5 satisfies:

$$\begin{aligned} \mathbb{E}_{(X, G, y) \sim \mathcal{D}} \left[\tilde{\ell}(f(X, G), y) \right] - \frac{1}{\beta N} \sum_{i=1}^N \tilde{\ell}(f(X_i, G_i), y_i) &\leq \frac{B}{2\beta(1-\beta)N} \left(\sum_{i=1}^l \frac{\|W^{(i)}\|_F^2 + \|U^{(i)}\|_F^2}{2\sigma_i^2} + \log \frac{1}{\delta} \right) \\ &\leq \frac{B}{2\beta(1-\beta)N} \left(\sum_{i=1}^l \frac{s_i^2 r_i^2}{\sigma_i^2} + \log \frac{1}{\delta} \right). \end{aligned} \quad (15)$$

The above is because \mathbf{W} and \mathbf{U} are inside the hypothesis set \mathcal{H} . For any $i = 1, \dots, l$, let

$$\alpha_i = \max_{(X, G, y) \sim \mathcal{D}} \text{Tr} \left[\mathbf{H}^{(i)}[\ell(f(X, G), y)] \right].$$

Lastly, we use $\sigma_i^2 \alpha_i$ above to upper bound E_4 . Combined with equations (14) and (15), with probability at least $1 - 2\delta$, we get

$$\begin{aligned} L(f) - \frac{1}{\beta} \hat{L}(f) &\leq \frac{C_2 \sqrt{2h^2 \log(C_3 N / \delta)}}{\sqrt{N}} \sum_{i=1}^l \sigma_i^2 + \left(1 + \frac{1}{\beta}\right) C_1 \sum_{i=1}^l \sigma_i^3 \\ &\quad + \frac{1}{2} \left(\frac{1}{\beta} - 1 \right) \sum_{i=1}^l \alpha_i \sigma_i^2 + \frac{B}{2\beta(1-\beta)N} \left(\sum_{i=1}^l \frac{s_i^2 r_i^2}{\sigma_i^2} + \log \frac{1}{\delta} \right). \end{aligned}$$

Next, we will select σ_i to minimize the last line above. One can verify that this is achieved when

$$\sigma_i^2 = \frac{s_i r_i}{1 - \beta} \sqrt{\frac{B}{\alpha_i N}}, \text{ for every } i = 1, 2, \dots, l.$$

With this setting of the noise variance, the gap between $L(f)$ and $\hat{L}(f)/\beta$ becomes:

$$\begin{aligned} L(f) - \frac{1}{\beta} \hat{L}(f) &\leq \frac{1}{\beta} \sum_{i=1}^l \sqrt{\frac{B \alpha_i s_i^2 r_i^2}{N}} + \frac{C_2 \sqrt{2h^2 \log(C_3 N / \delta)}}{\sqrt{N}} \sum_{i=1}^l \sigma_i^2 + \left(1 + \frac{1}{\beta}\right) C_1 \sum_{i=1}^l \sigma_i^3 + \frac{C}{2\beta(1-\beta)N} \log \frac{1}{\delta}. \end{aligned}$$

Let β be a fixed value close to 1 and independent of N and δ^{-1} ; let $\epsilon = (1 - \beta)/\beta$. We get

$$\begin{aligned} L(f) &\leq (1 + \epsilon) \hat{L}(f) + (1 + \epsilon) \sum_{i=1}^l \sqrt{\frac{B \alpha_i r_i^2 s_i^2}{N}} + \xi, \text{ where} \\ \xi &= \frac{C_2 \sqrt{2h^2 \log(C_3 N / \delta)}}{\sqrt{N}} \sum_{i=1}^l \sigma_i^2 + \left(1 + \frac{1}{\beta}\right) C_1 \sum_{i=1}^l \sigma_i^3 + \frac{C}{2\beta(1-\beta)N} \log \frac{1}{\delta}. \end{aligned}$$

Notice that ξ is of order $O(N^{-3/4} + \log(\delta^{-1})N^{-1}) \leq O(\log(\delta^{-1})/N^{3/4})$. Therefore, we have finished the proof of equation (5).

A.1.1 Proof of Proposition A.4

For any $j = 1, 2, \dots, l$, let $\tilde{H}^{(j)}$ be the perturbed network output after layer j , with perturbations given by $\Delta\mathbf{W}$ and $\Delta\mathbf{U}$. We show the following Lipschitz-continuity property for $H^{(j)}$.

Claim A.5. *Suppose that Assumption A.2 holds. For any $j = 1, \dots, l-1$, the change in the output of the j layer network $H^{(j)}$ with perturbation added to \mathbf{W} and \mathbf{U} can be bounded as follows:*

$$\left\| \tilde{H}^{(j)} - H^{(j)} \right\|_F \lesssim \sum_{t=1}^j \left(\left\| \Delta U^{(t)} \right\| + \left\| \Delta W^{(t)} \right\| \right). \quad (16)$$

Proof. We will prove using induction with respect to j . If $j = 1$, we have

$$\begin{aligned} & \left\| \phi_1 \left(X(U^{(1)} + \Delta U^{(1)}) + \rho_1(P_G \psi_1(X))(W^{(1)} + \Delta W^{(1)}) \right) - \phi_1 \left(XU^{(1)} + \rho_1(P_G \psi_1(X))W^{(1)} \right) \right\|_F \\ & \leq \kappa_0 \left\| X\Delta U^{(1)} + \rho_1(P_G \psi_1(X))\Delta W^{(1)} \right\|_F \lesssim \left\| \Delta U^{(1)} \right\| + \left\| \Delta W^{(1)} \right\|. \end{aligned}$$

Hence, we know that equation (16) will be correct when $j = 1$. Assuming that equation (16) is correct for any $j \geq 1$, the perturbation of layer $j+1$'s network output $H^{(j+1)}$ is less than

$$\begin{aligned} & \left\| \tilde{H}^{(j+1)} - H^{(j+1)} \right\|_F \\ & \leq \kappa_0 \left\| X\Delta U^{(j+1)} + \rho_{j+1}(P_G \psi_{j+1}(\tilde{H}^{(j)}))(W^{(j+1)} + \Delta W^{(j+1)}) - \rho_{j+1}(P_G \psi_{j+1}(H^{(j)}))W^{(j+1)} \right\|_F \\ & \lesssim \left\| \Delta U^{(j+1)} \right\| + \left\| \Delta W^{(j+1)} \right\| + \left\| \tilde{H}^{(j)} - H^{(j)} \right\|_F. \end{aligned}$$

Thus, we have finished the proof of the induction step.

Next, for any i and j , let $\frac{\partial \tilde{H}^{(j)}}{\partial W^{(i)}}$ be the perturbation of the partial derivative of $H^{(j)}$ with perturbations given by $\Delta\mathbf{W}$ and $\Delta\mathbf{U}$.

Claim A.6. *Suppose that Assumption A.2 holds. For any $j = 1, \dots, l-1$, the change in the Jacobian of the j -th layer's output $H^{(j)}$ with respect to $W^{(i)}$ and $U^{(i)}$ satisfies:*

$$\left\| \frac{\partial \tilde{H}^{(j)}}{\partial W^{(i)}} - \frac{\partial H^{(j)}}{\partial W^{(i)}} \right\|_F \lesssim \sum_{t=1}^j \left(\left\| \Delta U^{(t)} \right\| + \left\| \Delta W^{(t)} \right\| \right). \quad (17)$$

$$\left\| \frac{\partial \tilde{H}^{(j)}}{\partial U^{(i)}} - \frac{\partial H^{(j)}}{\partial U^{(i)}} \right\|_F \lesssim \sum_{t=1}^j \left(\left\| \Delta U^{(t)} \right\| + \left\| \Delta W^{(t)} \right\| \right). \quad (18)$$

Proof. We will consider a fixed $i = 1, \dots, l-1$ and take induction over $j = i, \dots, l-1$. We focus on the proof of equation (17), while the proof of equation (18) will be similar. To simplify the derivation, we use two notations for brevity. Let

$$F_j = P_G \psi_j(H^{(j-1)})W^{(j)} \text{ and } E_j = XU^{(j)} + \rho_j(F_j).$$

First, we consider the base case when $j = i$. By the chain rule, we have:

$$\begin{aligned} \left\| \frac{\partial \tilde{H}^{(i)}}{\partial W^{(i)}} - \frac{\partial H^{(i)}}{\partial W^{(i)}} \right\|_F &= \left\| \phi'_i(\tilde{E}_i) \odot \frac{\partial \tilde{E}_i}{\partial W^{(i)}} - \phi'_i(E_i) \odot \frac{\partial E_i}{\partial W^{(i)}} \right\|_F \\ &\lesssim \left\| \phi'_i(\tilde{E}_i) - \phi'_i(E_i) \right\|_F + \left\| \frac{\partial \tilde{E}_i}{\partial W^{(i)}} - \frac{\partial E_i}{\partial W^{(i)}} \right\|_F. \end{aligned}$$

From Claim A.5, we know

$$\left\| \phi'_i(\tilde{E}_i) - \phi'_i(E_i) \right\|_F \leq \kappa_1 \left\| \tilde{E}_i - E_i \right\|_F \lesssim \left\| \Delta W^{(i)} \right\| + \left\| \Delta U^{(i)} \right\|.$$

By the chain rule again, we get:

$$\begin{aligned} \left\| \frac{\partial \tilde{E}_i}{\partial W^{(i)}} - \frac{\partial E_i}{\partial W^{(i)}} \right\|_F &\lesssim \left\| \rho'_i(\tilde{F}_i) - \rho'_i(F_i) \right\|_F + \left\| \frac{\partial \tilde{F}_i}{\partial W^{(i)}} - \frac{\partial F_i}{\partial W^{(i)}} \right\|_F \lesssim \left\| \Delta W^{(i)} \right\| + \left\| \Delta U^{(i)} \right\|, \\ &\quad \text{(by Claim A.5 again)} \end{aligned}$$

Hence, we know that equation (17) will be correct when $j = i$. Assuming that equation (17) will be correct for any j up to $j \geq i$, we have

$$\begin{aligned} &\left\| \frac{\partial \tilde{H}^{(j+1)}}{\partial W^{(i)}} - \frac{\partial H^{(j+1)}}{\partial W^{(i)}} \right\|_F \\ &\lesssim \left\| \phi'_{j+1}(\tilde{E}_{j+1}) - \phi'_{j+1}(E_{j+1}) \right\|_F + \left\| \frac{\partial \tilde{E}_{j+1}}{\partial W^{(i)}} - \frac{\partial E_{j+1}}{\partial W^{(i)}} \right\|_F \\ &\lesssim \sum_{t=1}^{j+1} \left(\left\| \Delta U^{(t)} \right\| + \left\| \Delta W^{(t)} \right\| \right) + \left\| \rho'_{j+1}(\tilde{F}_{j+1}) - \rho'_{j+1}(F_{j+1}) \right\|_F + \left\| \frac{\partial \tilde{F}_{j+1}}{\partial W^{(i)}} - \frac{\partial F_{j+1}}{\partial W^{(i)}} \right\|_F \\ &\lesssim \sum_{t=1}^{j+1} \left(\left\| \Delta U^{(t)} \right\| + \left\| \Delta W^{(t)} \right\| \right) + \left\| \psi'_{j+1}(\tilde{H}^{(j)}) - \psi'_{j+1}(H^{(j)}) \right\|_F + \left\| \frac{\partial \tilde{H}^{(j)}}{\partial W^{(i)}} - \frac{\partial H^{(j)}}{\partial W^{(i)}} \right\|_F \\ &\lesssim \sum_{t=1}^{j+1} \left(\left\| \Delta U^{(t)} \right\| + \left\| \Delta W^{(t)} \right\| \right). \end{aligned} \quad \text{(by Claim A.5 and the induction step)}$$

The above steps all use Claim A.5. The last step additionally uses the induction hypothesis. From repeatedly applying the above beginning with $j = i$ along with the base case of equation (17), we conclude that equation (17) holds.

Next, we consider the base case for equation (18). For the base case $j = i$, from the chain rule, by Claim A.5, we get:

$$\left\| \frac{\partial \tilde{H}^{(i)}}{\partial U^{(i)}} - \frac{\partial H^{(i)}}{\partial U^{(i)}} \right\|_F \lesssim \left\| \phi'_i(\tilde{E}_i) - \phi'_i(E_i) \right\|_F + \left\| \frac{\partial \tilde{E}_i}{\partial U^{(i)}} - \frac{\partial E_i}{\partial U^{(i)}} \right\|_F \lesssim \left\| \Delta W^{(i)} \right\| + \left\| \Delta U^{(i)} \right\|.$$

Hence, we know that equation (18) will be correct when $j = i$. Assuming that equation (18) will be correct for any j up to $j \geq i$, we have

$$\begin{aligned} &\left\| \frac{\partial \tilde{H}^{(j+1)}}{\partial U^{(i)}} - \frac{\partial H^{(j+1)}}{\partial U^{(i)}} \right\|_F \lesssim \left\| \phi'_{j+1}(\tilde{E}_{j+1}) - \phi'_{j+1}(E_{j+1}) \right\|_F + \left\| \frac{\partial \tilde{E}_{j+1}}{\partial U^{(i)}} - \frac{\partial E_{j+1}}{\partial U^{(i)}} \right\|_F \\ &\lesssim \sum_{t=1}^{j+1} \left(\left\| \Delta U^{(t)} \right\| + \left\| \Delta W^{(t)} \right\| \right) + \left\| \rho'_{j+1}(\tilde{F}_{j+1}) - \rho'_{j+1}(F_{j+1}) \right\|_F + \left\| \frac{\partial \tilde{F}_{j+1}}{\partial U^{(i)}} - \frac{\partial F_{j+1}}{\partial U^{(i)}} \right\|_F \\ &\lesssim \sum_{t=1}^{j+1} \left(\left\| \Delta U^{(t)} \right\| + \left\| \Delta W^{(t)} \right\| \right) + \left\| \psi'_{j+1}(\tilde{H}^{(j)}) - \psi'_{j+1}(H^{(j)}) \right\|_F + \left\| \frac{\partial \tilde{H}^{(j)}}{\partial U^{(i)}} - \frac{\partial H^{(j)}}{\partial U^{(i)}} \right\|_F \\ &\lesssim \sum_{t=1}^{j+1} \left(\left\| \Delta U^{(t)} \right\| + \left\| \Delta W^{(t)} \right\| \right). \end{aligned} \quad \text{(by Claim A.5 and the induction step)}$$

The second and third steps are based on Claim A.5. From repeatedly applying the above beginning with $j = i$ along with the base case of equation (18), we conclude that equation (18) holds. The proof of claim A.6 is complete.

Proof of Proposition A.4. We will consider a fixed $i = 1, \dots, l-1$ and take induction over $j = i, \dots, l-1$. We focus on the proof of equation (12), while the proof of equation (13) will be similar. To simplify the derivation, we use two notations for brevity. Let

$$F_j = P_G \psi_j(H^{(j-1)}) W^{(j)} \text{ and } E_j = X U^{(j)} + \rho_j(F_j).$$

First, we consider the base case when $j = i$. By the chain rule, we have: We use the chain rule to get:

$$\frac{\partial^2 H^{(i)}}{\partial (W_{p,q}^{(i)})^2} = \phi_i''(E_i) \odot \frac{\partial E_i}{\partial W_{p,q}^{(i)}} \odot \frac{\partial E_i}{\partial W_{p,q}^{(i)}} + \phi_i'(E_i) \odot \rho_i''(F_i) \odot \frac{\partial F_i}{\partial W_{p,q}^{(i)}} \odot \frac{\partial F_i}{\partial W_{p,q}^{(i)}}.$$

Hence, the Frobenius norm of the Hessian of $H^{(i)}$ with respect to W_i under perturbation on W and U turns to

$$\begin{aligned} \left\| \mathbf{H}_{\mathbf{W}}^{(i)}[\tilde{H}^{(i)}] - \mathbf{H}_{\mathbf{W}}^{(i)}[H^{(i)}] \right\|_F &\lesssim \left\| \phi_i''(\tilde{E}_i) - \phi_i''(E_i) \right\|_F + \left\| \frac{\partial \tilde{E}_i}{\partial W^{(i)}} - \frac{\partial E_i}{\partial W^{(i)}} \right\|_F + \left\| \phi_i'(\tilde{E}_i) - \phi_i'(E_i) \right\|_F \\ &\quad + \left\| \rho_i''(\tilde{F}_i) - \rho_i''(F_i) \right\|_F + \left\| \frac{\partial \tilde{F}_i}{\partial W^{(i)}} - \frac{\partial F_i}{\partial W^{(i)}} \right\|_F. \end{aligned}$$

From Claim A.5, we know

$$\begin{aligned} \left\| \phi_i''(\tilde{E}_i) - \phi_i''(E_i) \right\|_F &\leq \kappa_2 \left\| \tilde{E}_i - E_i \right\|_F \lesssim \left\| \Delta W^{(i)} \right\| + \left\| \Delta U^{(i)} \right\|, \\ \left\| \phi_i'(\tilde{E}_i) - \phi_i'(E_i) \right\|_F &\leq \kappa_1 \left\| \tilde{E}_i - E_i \right\|_F \lesssim \left\| \Delta W^{(i)} \right\| + \left\| \Delta U^{(i)} \right\|, \\ \left\| \rho_i''(\tilde{F}_i) - \rho_i''(F_i) \right\|_F &\leq \kappa_2 \left\| \tilde{F}_i - F_i \right\|_F \lesssim \left\| \Delta W^{(i)} \right\| + \left\| \Delta U^{(i)} \right\|. \end{aligned}$$

From Claim A.6, we have

$$\begin{aligned} \left\| \frac{\partial \tilde{E}_i}{\partial W^{(i)}} - \frac{\partial E_i}{\partial W^{(i)}} \right\|_F &\lesssim \left\| \Delta W^{(i)} \right\| + \left\| \Delta U^{(i)} \right\|, \\ \left\| \frac{\partial \tilde{F}_i}{\partial W^{(i)}} - \frac{\partial F_i}{\partial W^{(i)}} \right\|_F &\lesssim \left\| \Delta W^{(i)} \right\| + \left\| \Delta U^{(i)} \right\|. \end{aligned}$$

Hence, we know that equation (12) will be correct when $j = i$. Assuming that equation (12) will be correct for any j up to $j \geq i$, we can get the following steps, by taking another derivative of the first-order derivative, we can get the following steps:

$$\begin{aligned} \frac{\partial^2 H^{(j+1)}}{\partial (W_{p,q}^{(i)})^2} &= \phi_{j+1}''(E_{j+1}) \odot \frac{\partial E_{j+1}}{\partial W_{p,q}^{(i)}} \odot \frac{\partial E_{j+1}}{\partial W_{p,q}^{(i)}} + \phi_{j+1}'(E_{j+1}) \odot \rho_{j+1}''(F_{j+1}) \odot \frac{\partial F_{j+1}}{\partial W_{p,q}^{(i)}} \odot \frac{\partial F_{j+1}}{\partial W_{p,q}^{(i)}} \\ &\quad + \phi_{j+1}'(E_{j+1}) \odot \rho_{j+1}'(F_{j+1}) \odot P_G \left(\psi_{j+1}''(H^{(j)}) \odot \frac{\partial H^{(j)}}{\partial W_{p,q}^{(i)}} \odot \frac{\partial H^{(j)}}{\partial W_{p,q}^{(i)}} + \psi_{j+1}'(H^{(j)}) \odot \frac{\partial^2 H^{(j)}}{\partial (W_{p,q}^{(i)})^2} \right) W^{(j+1)}. \end{aligned}$$

Thus, the Frobenius norm of the Hessian of $H^{(j+1)}$ with respect to $W^{(i)}$ satisfies:

$$\begin{aligned}
\left\| \mathbf{H}_{\mathbf{W}}^{(i)}[\tilde{H}^{(j+1)}] - \mathbf{H}_{\mathbf{W}}^{(i)}[H^{(j+1)}] \right\|_F &\lesssim \underbrace{\left\| \phi''_{j+1}(\tilde{E}_{j+1}) - \phi''_{j+1}(E_{j+1}) \right\|_F}_{A_1} + \underbrace{\left\| \frac{\partial \tilde{E}_{j+1}}{\partial W^{(i)}} - \frac{\partial E_{j+1}}{\partial W^{(i)}} \right\|_F}_{B_1} \\
&+ \underbrace{\left\| \phi'_{j+1}(\tilde{E}_{j+1}) - \phi'_{j+1}(E_{j+1}) \right\|_F}_{A_2} + \underbrace{\left\| \rho''_{j+1}(\tilde{F}_{j+1}) - \rho''_{j+1}(F_{j+1}) \right\|_F}_{A_3} \\
&+ \underbrace{\left\| \frac{\partial \tilde{F}_{j+1}}{\partial W^{(i)}} - \frac{\partial F_{j+1}}{\partial W^{(i)}} \right\|_F}_{B_2} + \underbrace{\left\| \rho'_{j+1}(\tilde{F}_{j+1}) - \rho'_{j+1}(F_{j+1}) \right\|_F}_{A_4} \\
&+ \underbrace{\left\| \psi''_{j+1}(\tilde{H}^{(j)}) - \psi''_{j+1}(H^{(j)}) \right\|_F}_{A_5} + \underbrace{\left\| \frac{\partial \tilde{H}^{(j)}}{\partial W^{(i)}} - \frac{\partial H^{(j)}}{\partial W^{(i)}} \right\|_F}_{B_3} \\
&+ \underbrace{\left\| \psi'_{j+1}(\tilde{H}^{(j)}) - \psi'_{j+1}(H^{(j)}) \right\|_F}_{A_6} + \underbrace{\left\| \mathbf{H}_{\mathbf{W}}^{(i)}[\tilde{H}^{(j)}] - \mathbf{H}_{\mathbf{W}}^{(i)}[H^{(j)}] \right\|_F}_{C_1}.
\end{aligned}$$

Similarly, by Claim A.5, we get

$$A_i \lesssim \sum_{t=1}^{j+1} \left(\left\| \Delta W^{(t)} \right\| + \left\| \Delta U^{(t)} \right\| \right), \text{ for } 1 \leq i \leq 6.$$

By Claim A.6, we get

$$B_i \lesssim \sum_{t=1}^{j+1} \left(\left\| \Delta W^{(t)} \right\| + \left\| \Delta U^{(t)} \right\| \right), \text{ for } 1 \leq i \leq 3.$$

By the induction hypothesis, C_1 is also less than the above quantity. From repeatedly applying the above beginning with $j = i$ along with the base case of equation (12), we conclude that equation (12) holds.

Next, we consider the base case for equation (13). For the base case $j = i$, from the chain rule, we get:

$$\begin{aligned}
\left\| \mathbf{H}_{\mathbf{U}}^{(i)}[\tilde{H}^{(i)}] - \mathbf{H}_{\mathbf{U}}^{(i)}[H^{(i)}] \right\|_F &\lesssim \left\| \phi''_i(\tilde{E}_i) - \phi''_i(E_i) \right\|_F + \left\| \frac{\partial \tilde{E}_i}{\partial U^{(i)}} - \frac{\partial E_i}{\partial U^{(i)}} \right\|_F \\
&\lesssim \kappa_2 \left\| \tilde{E}_i - E_i \right\|_F + \left\| \Delta W^{(i)} \right\| + \left\| \Delta U^{(i)} \right\| \quad (\text{by Claim A.6}) \\
&\lesssim \left\| \Delta W^{(i)} \right\| + \left\| \Delta U^{(i)} \right\|. \quad (\text{by Claim A.5})
\end{aligned}$$

Hence, we know that equation (13) will be correct when $j = i$. Assuming that equation (13) will be correct for any j up to $j \geq i$, we obtain the induction step similar to the proof of equation (12), by Claim A.5, Claim A.6, and the induction hypothesis, we conclude that equation (13) holds.

A.2 Proof for message passing graph neural networks

Next, we present proof for message-passing graph neural networks. First, in Appendix A.2.1, we derive the trace bound, which separates the trace of the Hessian matrix into each entry of the weight

matrices. Then in Appendix A.2.2 and A.2.3, we provide bounds on the first-order and second-order derivatives of the Hessian matrix. Last, in Appendix A.2.4, building on these results, we finish the proof of Theorem 3.1.

A.2.1 Proof of Lemma 4.3

Proof of Lemma 4.3. Notice that $f(X, G) = H^{(l)}$. Recall that in each layer for $1 \leq i \leq l-1$, there are two weight matrices, a d_{i-1} by d_i matrix denoted as $W^{(i)}$, and a d_0 by $U^{(i)}$ matrix denoted as $U^{(i)}$. To deal with the trace of the Hessian $\mathbf{H}^{(i)}$, we first notice that there are two parts in the trace:

$$\left| \text{Tr} [\mathbf{H}^{(i)}[\ell(H^{(l)}, y)]] \right| \leq \underbrace{\sum_{p=1}^{d_{i-1}} \sum_{q=1}^{d_i} \frac{\partial^2 \ell(H^{(l)}, y)}{\partial (W_{p,q}^{(i)})^2}}_{T_1} + \underbrace{\sum_{p=1}^{d_0} \sum_{q=1}^{d_i} \frac{\partial^2 \ell(H^{(l)}, y)}{\partial (U_{p,q}^{(i)})^2}}_{T_2}.$$

We can inspect T_1 and T_2 in the above step separately. First, we expand out the second-order derivatives in T_1 . This will involve two terms by the chain rule.

$$\begin{aligned} T_1 &= \left| \sum_{p=1}^{d_{i-1}} \sum_{q=1}^{d_i} \left\langle \frac{\partial \ell(H^{(l)}, y)}{\partial H^{(l)}}, \frac{\partial^2 H^{(l)}}{\partial (W_{p,q}^{(i)})^2} \right\rangle \right| + \left| \sum_{p=1}^{d_{i-1}} \sum_{q=1}^{d_i} \left\langle \frac{\partial^2 \ell(H^{(l)}, y)}{\partial (H^{(l)})^2} \frac{\partial H^{(l)}}{\partial W_{p,q}^{(i)}}, \frac{\partial H^{(l)}}{\partial W_{p,q}^{(i)}} \right\rangle \right| \\ &\leq \sum_{p=1}^{d_{i-1}} \sum_{q=1}^{d_i} \left\| \frac{\partial \ell(H^{(l)}, y)}{\partial H^{(l)}} \right\| \left\| \frac{\partial^2 H^{(l)}}{\partial (W_{p,q}^{(i)})^2} \right\| + \sum_{p=1}^{d_{i-1}} \sum_{q=1}^{d_i} \left\| \frac{\partial^2 \ell(H^{(l)}, y)}{\partial (H^{(l)})^2} \right\| \left\| \frac{\partial H^{(l)}}{\partial W_{p,q}^{(i)}} \right\|^2 \\ &\leq \kappa_0 \sqrt{k} \sum_{p=1}^{d_{i-1}} \sum_{q=1}^{d_i} \left\| \frac{\partial^2 H^{(l)}}{\partial (W_{p,q}^{(i)})^2} \right\| + \kappa_1 k \sum_{p=1}^{d_{i-1}} \sum_{q=1}^{d_i} \left\| \frac{\partial H^{(l)}}{\partial W_{p,q}^{(i)}} \right\|^2. \end{aligned} \tag{19}$$

The last step is because $\ell(\cdot)$ is κ_0 -Lipschitz continuous and $\ell'(\cdot)$ is κ_1 -Lipschitz continuous, under Assumption A.2. Thus, the Euclidean norm of $\frac{\partial \ell(H^{(l)}, y)}{\partial H^{(l)}}$ is at most $\kappa_0 \sqrt{k}$, since $H^{(l)}$ is a k -dimensional vector. Recall from step (2) that $H^{(l)} = \frac{1}{n} \mathbf{1}_n^\top H^{(l-1)} W^{(l)}$. Hence, we have

$$\begin{aligned} \left\| \frac{\partial H^{(l)}}{\partial W_{p,q}^{(i)}} \right\| &= \left\| \frac{1}{n} \mathbf{1}_n^\top \frac{\partial H^{(l-1)}}{\partial W_{p,q}^{(i)}} W^{(l)} \right\| \\ &\leq \left\| \frac{1}{n} \mathbf{1}_n^\top \right\| \left\| \frac{\partial H^{(l-1)}}{\partial W_{p,q}^{(i)}} W^{(l)} \right\| \leq \frac{1}{\sqrt{n}} \left\| \frac{\partial H^{(l-1)}}{\partial W_{p,q}^{(i)}} \right\| \|W^{(l)}\|. \end{aligned} \tag{20}$$

In a similar vein, the Euclidean norm of $\frac{\partial^2 \ell(H^{(l)}, y)}{\partial (H^{(l)})^2}$ is at most $\kappa_1 k$, since the second-order derivatives become a k by k matrix. Then, we get

$$\begin{aligned} \left\| \frac{\partial^2 H^{(l)}}{\partial (W_{p,q}^{(i)})^2} \right\| &= \left\| \frac{1}{n} \mathbf{1}_n^\top \frac{\partial^2 H^{(l-1)}}{\partial (W_{p,q}^{(i)})^2} W^{(l)} \right\| \\ &\leq \left\| \frac{1}{n} \mathbf{1}_n^\top \right\| \left\| \frac{\partial^2 H^{(l-1)}}{\partial (W_{p,q}^{(i)})^2} W^{(l)} \right\| \leq \frac{1}{\sqrt{n}} \left\| \frac{\partial^2 H^{(l-1)}}{\partial (W_{p,q}^{(i)})^2} \right\| \|W^{(l)}\|. \end{aligned} \tag{21}$$

After substituting equations (20) and (21) into equation (19), we get:

$$\begin{aligned} T_1 &\leq \frac{\kappa_0 \sqrt{k}}{\sqrt{n}} \|W^{(l)}\| \sum_{p=1}^{d_{i-1}} \sum_{q=1}^{d_i} \left\| \frac{\partial^2 H^{(l-1)}}{\partial (W_{p,q}^{(i)})^2} \right\| + \frac{\kappa_1 k}{n} \|W^{(l)}\|^2 \sum_{p=1}^{d_{i-1}} \sum_{q=1}^{d_i} \left\| \frac{\partial H^{(l-1)}}{\partial W_{p,q}^{(i)}} \right\|^2. \\ &\leq \frac{\kappa_0 \sqrt{k}}{\sqrt{n}} \|W^{(l)}\| \sum_{p=1}^{d_{i-1}} \sum_{q=1}^{d_i} \left\| \frac{\partial^2 H^{(l-1)}}{\partial (W_{p,q}^{(i)})^2} \right\|_F + \frac{\kappa_1 k}{n} \|W^{(l)}\|^2 \sum_{p=1}^{d_{i-1}} \sum_{q=1}^{d_i} \left\| \frac{\partial H^{(l-1)}}{\partial W_{p,q}^{(i)}} \right\|_F^2. \end{aligned}$$

The proof for the case of T_2 concerning $U^{(i)}$ follows the same steps as above. Without belaboring all the details, one can get that

$$T_2 \leq \frac{\kappa_0 \sqrt{k}}{\sqrt{n}} \|W^{(l)}\| \sum_{p=1}^{d_0} \sum_{q=1}^{d_i} \left\| \frac{\partial^2 H^{(l-1)}}{\partial (U_{p,q}^{(i)})^2} \right\|_F + \frac{\kappa_1 k}{n} \|W^{(l)}\|^2 \sum_{p=1}^{d_0} \sum_{q=1}^{d_i} \left\| \frac{\partial H^{(l-1)}}{\partial U_{p,q}^{(i)}} \right\|_F^2. \quad (22)$$

This completes the proof of Lemma 4.3.

A.2.2 Dealing with first-order derivatives

Based on Lemma 4.3, the analysis involves two parts, one on the first-order derivatives of $H^{(j)}$ for all layers j , and the other on the second-order derivatives of $H^{(j)}$ for all layers j .

Proposition A.7. *In the setting of Theorem 3.1, the first-order derivative of $H^{(j)}$ with respect to $W^{(i)}$ and $U^{(i)}$ satisfies the following, for any $i = 1, \dots, l-1$ and $j \geq i$:*

$$\left\| \frac{\partial H^{(j)}}{\partial W^{(i)}} \right\|_F \leq \kappa_0^{3(j-i+1)} \sqrt{d_i} \|P_G\|^{j-i+1} \|H^{(i-1)}\|_F \prod_{t=i+1}^j \|W^{(t)}\|, \quad (23)$$

$$\left\| \frac{\partial H^{(j)}}{\partial U^{(i)}} \right\|_F \leq \kappa_0^{3(j-i)+1} \sqrt{d_i} \|P_G\|^{j-i+1} \|X\|_F \prod_{t=i+1}^j \|W^{(t)}\|. \quad (24)$$

Proof. We will consider a fixed $i = 1, \dots, l-1$ and take induction over $j = i, \dots, l-1$. We focus on the proof of equation (23), while the proof of equation (24) will be similar. First, we consider the base case when $j = i$. Let $W_{p,q}^{(i)}$ be the (p, q) -th entry of $W^{(i)}$, for any valid indices p and q . Recall that $\phi_i(\cdot)$ is κ_0 -Lipschitz continuous from Assumption A.2, for any $i = 1, \dots, l-1$. Therefore,

$$\|\phi_i'(x)\|_\infty \leq \kappa_0, \quad \|\psi_i'(x)\|_\infty \leq \kappa_0, \quad \text{and} \quad \|\rho_i'(x)\|_\infty \leq \kappa_0. \quad (25)$$

For each (p, q) -entry of $W^{(i)}$, by the chain rule, we have:

$$\begin{aligned} \left\| \frac{\partial H^{(i)}}{\partial W_{p,q}^{(i)}} \right\|_F &= \left\| \phi_i'(XU^{(i)} + \rho_i(P_G \psi_i(H^{(i-1)})W^{(i)})) \odot \frac{\partial(XU^{(i)} + \rho_i(P_G \psi_i(H^{(i-1)})W^{(i)}))}{\partial W_{p,q}^{(i)}} \right\|_F \quad (26) \\ &\leq \kappa_0 \left\| \frac{\partial \rho_i(P_G \psi_i(H^{(i-1)})W^{(i)})}{\partial W_{p,q}^{(i)}} \right\|_F \quad (\text{by equation (25)}) \\ &= \kappa_0 \left\| \rho_i'(P_G \psi_i(H^{(i-1)})W^{(i)}) \odot \frac{\partial(P_G \psi_i(H^{(i-1)})W^{(i)})}{W_{p,q}^{(i)}} \right\|_F \\ &\leq \kappa_0^2 \left\| \frac{\partial(P_G \psi_i(H^{(i-1)})W^{(i)})}{\partial W_{p,q}^{(i)}} \right\|_F. \quad (\text{again by equation (25)}) \end{aligned}$$

Notice that only the q -th column of the derivative $P_G \psi_i(H^{(i-1)}) W^{(i)}$ is nonzero, which is equal to the p 'th column of $P_G \psi_i(H^{(i-1)})$. Thus, the Jacobian of $H^{(i)}$ over $W^{(i)}$ satisfies:

$$\begin{aligned} \left\| \frac{\partial H^{(i)}}{\partial W^{(i)}} \right\|_F &= \sqrt{\sum_{p=1}^{d_{i-1}} \sum_{q=1}^{d_i} \left\| \frac{\partial H^{(i)}}{\partial W_{p,q}^{(i)}} \right\|_F^2} \\ &\leq \kappa_0^2 \sqrt{\sum_{p=1}^{d_{i-1}} \sum_{q=1}^{d_i} \left\| \frac{\partial (P_G \psi_i(H^{(i-1)}) W^{(i)})}{W_{p,q}^{(i)}} \right\|_F^2} = \kappa_0^2 \sqrt{d_i} \left\| P_G \psi_i(H^{(i-1)}) \right\|_F. \end{aligned} \quad (27)$$

Therefore, the above equation (27) implies that equation (23) holds in the base case. Next, we consider the induction step from layer j to layer $j+1$. The derivative of $H^{(j+1)}$ with respect to $W_{p,q}^{(i)}$ satisfies:

$$\begin{aligned} &\left\| \frac{\partial H^{(j+1)}}{\partial W_{p,q}^{(i)}} \right\|_F \\ &= \left\| \phi'_{j+1}(XU^{(j+1)} + \rho_{j+1}(P_G \psi_{j+1}(H^{(j)}) W^{(j+1)})) \odot \frac{\partial (XU^{(j+1)} + \rho_{j+1}(P_G \psi_{j+1}(H^{(j)}) W^{(j+1)}))}{\partial W_{p,q}^{(i)}} \right\|_F \\ &\leq \kappa_0 \left\| \frac{\partial \rho_{j+1}(P_G \psi_{j+1}(H^{(j)}) W^{(j+1)})}{\partial W_{p,q}^{(i)}} \right\|_F \quad (\text{by equation (25)}) \\ &\leq \kappa_0 \left\| \rho'_{j+1}(P_G \psi_{j+1}(H^{(j)}) W^{(j+1)}) \odot \frac{\partial (P_G \psi_{j+1}(H^{(j)}) W^{(j+1)})}{\partial W_{p,q}^{(i)}} \right\|_F \\ &\leq \kappa_0^2 \left\| P_G \frac{\partial \psi_{j+1}(H^{(j)})}{\partial W_{p,q}^{(i)}} W^{(j+1)} \right\|_F \quad (\text{again by equation (25)}) \end{aligned}$$

By applying equation (25) w.r.t. ψ'_{j+1} , The above is less than:

$$\kappa_0^2 \|P_G\| \left\| \psi'_{j+1}(H^{(j)}) \odot \frac{\partial H^{(j)}}{\partial W_{p,q}^{(i)}} \right\|_F \|W^{(j+1)}\| \leq \kappa_0^3 \|P_G\| \|W^{(j+1)}\| \left\| \frac{\partial H^{(j)}}{\partial W_{p,q}^{(i)}} \right\|_F.$$

Hence, the Jacobian of $H^{(j+1)}$ with respect to $W^{(i)}$ satisfies:

$$\left\| \frac{\partial H^{(j+1)}}{\partial W^{(i)}} \right\|_F \leq \kappa_0^3 \|P_G\| \|W^{(j+1)}\| \left\| \frac{\partial H^{(j)}}{\partial W^{(i)}} \right\|_F.$$

From repeatedly applying the above beginning with $j = i$ along with the base case of equation (27), we conclude that equation (23) holds.

Next, we consider the base case for equation (24). For each (p, q) -th entry of $U^{(i)}$, from the chain rule we get:

$$\begin{aligned} \left\| \frac{\partial H^{(i)}}{\partial U_{p,q}^{(i)}} \right\|_F &= \left\| \phi'_i \left(XU^{(i)} + \rho_i(P_G \psi_i(H^{(i-1)}) W^{(i)}) \right) \odot \frac{\partial (XU^{(i)} + \rho_i(P_G \psi_i(H^{(i-1)}) W^{(i)}))}{\partial U_{p,q}^{(i)}} \right\|_F \\ &\leq \kappa_0 \left\| \frac{\partial (XU^{(i)})}{\partial U_{p,q}^{(i)}} \right\|_F. \end{aligned} \quad (\text{by equation (25)})$$

Therefore, by summing over $p = 1, \dots, d_0$ and $q = 1, \dots, d_i$, we get:

$$\begin{aligned} \left\| \frac{\partial H^{(i)}}{\partial U^{(i)}} \right\|_F &= \sqrt{\sum_{p=1}^{d_0} \sum_{q=1}^{d_i} \left\| \frac{\partial H^{(i)}}{\partial U_{p,q}^{(i)}} \right\|_F^2} \\ &\leq \kappa_0 \sqrt{\sum_{p=1}^{d_0} \sum_{q=1}^{d_i} \left\| \frac{\partial (XU^{(i)})}{\partial U_{p,q}^{(i)}} \right\|_F^2} = \kappa_0 \sqrt{d_i} \|X\|_F. \end{aligned} \quad (28)$$

Going from layer i to layer $j+1$, the derivative of $H^{(j+1)}$ with respect to $U_{p,q}^{(i)}$ satisfies:

$$\begin{aligned} &\left\| \frac{\partial H^{(j+1)}}{\partial U_{p,q}^{(i)}} \right\|_F \\ &= \left\| \phi'_{j+1}(XU^{(j+1)} + \rho_{j+1}(P_G \psi_{j+1}(H^{(j)}) W^{(j+1)})) \odot \frac{\partial (XU^{(j+1)} + \rho_{j+1}(P_G \psi_{j+1}(H^{(j)}) W^{(j+1)}))}{\partial U_{p,q}^{(i)}} \right\|_F \\ &\leq \kappa_0 \left\| \frac{\partial \rho_{j+1}(P_G \psi_{j+1}(H^{(j)}) W^{(j+1)})}{\partial U_{p,q}^{(i)}} \right\|_F \quad (\text{by equation (25) w.r.t. } \phi'_{j+1}) \\ &\leq \kappa_0^3 \|P_G\| \|W^{(j+1)}\| \left\| \frac{\partial H^{(j)}}{\partial U_{p,q}^{(i)}} \right\|_F. \quad (\text{by equation (25) w.r.t. } \rho'_{j+1}, \psi'_{j+1}) \end{aligned}$$

Hence, the Jacobian of $H^{(j+1)}$ with respect to $U^{(i)}$ satisfies:

$$\left\| \frac{\partial H^{(j+1)}}{\partial U^{(i)}} \right\|_F \leq \kappa_0^3 \|P_G\| \|W^{(j+1)}\| \left\| \frac{\partial H^{(j)}}{\partial U^{(i)}} \right\|_F.$$

By repeatedly applying the above step beginning with the base case of equation (28), we have proved that equation (24) holds. The proof of Proposition A.7 is complete.

A.2.3 Deal with second-order derivatives

In the second part towards showing Theorem 3.1 for MPNNs, we look at second-order derivatives of the embeddings. This will appear later when we deal with the trace of the Hessian. A fact that we will use throughout the proof is

$$\|\phi''_i(x)\|_\infty \leq \kappa_1, \quad \|\psi''_i(x)\|_\infty \leq \kappa_1, \quad \text{and} \quad \|\rho''_i(x)\|_\infty \leq \kappa_1, \quad (29)$$

for any x and $i = 1, \dots, l-1$. This is because ϕ'_i, ψ'_i , and ρ'_i are all κ_1 -Lipschitz continuous from Assumption A.2.

Proposition A.8. *In the setting of Theorem 3.1, the second-order derivative of $H^{(l)}$ with respect to $W^{(i)}$ and $U^{(i)}$ satisfies the following, for any $i = 1, \dots, l-1$ and any $j = i, \dots, l-1$:*

$$\sum_{p=1}^{d_{i-1}} \sum_{q=1}^{d_i} \left\| \frac{\partial^2 H^{(j)}}{\partial (W_{p,q}^{(i)})^2} \right\|_F \leq C_{i,j} \kappa_1 d_i \max(\|P_G\|^{j-i+2}, \|P_G\|^{2(j-i+1)}) \|H^{(i-1)}\|_F^2 \prod_{t=i+1}^j s_t^2, \quad (30)$$

$$\sum_{p=1}^{d_{i-1}} \sum_{q=1}^{d_i} \left\| \frac{\partial^2 H^{(j)}}{\partial (U_{p,q}^{(i)})^2} \right\|_F \leq \hat{C}_{i,j} \kappa_1 d_i \max(\|P_G\|^{j-i}, \|P_G\|^{2(j-i)}) \|X\|_F^2 \prod_{t=i+1}^j s_t^2, \quad (31)$$

where $C_{i,j}$

$$C_{i,j} = \begin{cases} \kappa_0^{3(j-i+1)} \frac{\kappa_0^{3(j-i)+2} - 1}{\kappa_0 - 1}, & \kappa_0 \neq 1, \\ 3(j-i) + 2, & \kappa_0 = 1, \end{cases}$$

and $\hat{C}_{i,j}$

$$\hat{C}_{i,j} = \begin{cases} \kappa_0^{3(j-i)} \frac{\kappa_0^{3(j-i)+1} - 1}{\kappa_0 - 1}, & \kappa_0 \neq 1, \\ 3(j-i) + 1, & \kappa_0 = 1. \end{cases}$$

are fixed constants that depend on the Lipschitz-continuity of the activation mappings.

Proof. First, we will consider equation (30). To simplify the derivation, we introduce two notations for brevity. Let

$$F_j = P_G \psi_j(H^{(j-1)}) W^{(j)} \text{ and } E_j = X U^{(j)} + \rho_j(F_j).$$

In the base case when $j = i$, from the first-order derivative in equation (26), we use the chain rule to get:

$$\frac{\partial^2 H^{(i)}}{\partial (W_{p,q}^{(i)})^2} = \phi_i''(E_i) \odot \frac{\partial E_i}{\partial W_{p,q}^{(i)}} \odot \frac{\partial E_i}{\partial W_{p,q}^{(i)}} + \phi_i'(E_i) \odot \rho_i''(F_i) \odot \frac{\partial F_i}{\partial W_{p,q}^{(i)}} \odot \frac{\partial F_i}{\partial W_{p,q}^{(i)}}. \quad (32)$$

Using equation (29), the maximum entries of $\phi_i''(\cdot), \rho_i''(\cdot)$ are at most κ_1 . Using equation (25), the maximum entry of $\phi_i'(\cdot)$ is at most κ_0 . Notice that the derivative of E_i can be reduced to the derivative of F_i as follows:

$$\left\| \frac{\partial E_i}{\partial W_{p,q}^{(i)}} \right\|_F^2 = \left\| \rho_i'(F_i) \odot \frac{\partial F_i}{\partial W_{p,q}^{(i)}} \right\|_F^2 \leq \kappa_0^2 \left\| \frac{\partial F_i}{\partial W_{p,q}^{(i)}} \right\|_F^2. \quad (33)$$

Therefore, based on the conditions for first- and second-order derivatives (cf. (25) and (29)), the Frobenius norm of the above equation (32) is at most:

$$\left\| \frac{\partial^2 H^{(i)}}{\partial (W_{p,q}^{(i)})^2} \right\|_F \leq \kappa_1 \left\| \frac{\partial E_i}{\partial W_{p,q}^{(i)}} \right\|_F^2 + \kappa_0 \kappa_1 \left\| \frac{\partial F_i}{\partial W_{p,q}^{(i)}} \right\|_F^2 \leq (\kappa_0 + 1) \kappa_0 \kappa_1 \left\| \frac{\partial F_i}{\partial W_{p,q}^{(i)}} \right\|_F^2.$$

Notice that the derivative of F_i with respect to $W_{p,q}^{(i)}$ is nonzero only in the q -th column of F_i , and is equal to the p -th column of $P_G g_i(H^{(i-1)})$. Therefore, by summing over $p = 1, \dots, d_{i-1}$ and $q = 1, \dots, d_i$, we get:

$$\sum_{p=1}^{d_{i-1}} \sum_{q=1}^{d_i} \left\| \frac{\partial F_i}{\partial (W_{p,q}^{(i)})^2} \right\|_F^2 \leq d_i \left\| P_G \psi_i(H^{(i-1)}) \right\|_F^2.$$

Therefore, we have derived the base case when $j = i$ as:

$$\left\| \frac{\partial^2 H^{(i)}}{\partial (W_{p,q}^{(i)})^2} \right\|_F \leq (\kappa_0 + 1) \kappa_0^3 \kappa_1 d_i \|P_G\|^2 \left\| H^{(i-1)} \right\|_F^2. \quad (34)$$

Next, we consider the induction step from layer j to layer $j+1$. This step is similar to the base case but also differs since $H^{(j)}$ is now dependent on $W^{(i)}$. Recall that the second-order derivatives satisfy equation (29). Based on the Lipschitz-continuity conditions, the Frobenius norm of the second-order derivatives satisfies:

$$\left\| \frac{\partial^2 H^{(j+1)}}{\partial (W_{p,q}^{(i)})^2} \right\|_F \quad (35)$$

$$\begin{aligned} &\leq \kappa_1 \left\| \frac{\partial E_{j+1}}{\partial W_{p,q}^{(i)}} \right\|_F^2 + \kappa_0 \kappa_1 \left\| \frac{\partial F_{j+1}}{\partial W_{p,q}^{(i)}} \right\|_F^2 + \kappa_0^2 \|P_G\| \|W^{(j+1)}\| \left(\kappa_1 \left\| \frac{\partial H^{(j)}}{\partial W_{p,q}^{(i)}} \right\|_F^2 + \kappa_0 \left\| \frac{\partial^2 H^{(j)}}{\partial (W_{p,q}^{(i)})^2} \right\|_F \right) \\ &\leq (\kappa_0 + 1) \kappa_0 \kappa_1 \left\| \frac{\partial F_{j+1}}{\partial W_{p,q}^{(i)}} \right\|_F^2 + \kappa_0^2 \|P_G\| \|W^{(j+1)}\| \left(\kappa_1 \left\| \frac{\partial H^{(j)}}{\partial W_{p,q}^{(i)}} \right\|_F^2 + \kappa_0 \left\| \frac{\partial^2 H^{(j)}}{\partial (W_{p,q}^{(i)})^2} \right\|_F \right). \end{aligned} \quad (36)$$

The last step follows similarly as equation (33). For the derivative of F_{j+1} , using the chain rule, we get:

$$\begin{aligned} \left\| \frac{\partial F_{j+1}}{\partial W_{p,q}^{(i)}} \right\|_F^2 &= \left\| P_G \frac{\partial \psi_{j+1}(H^{(j)})}{\partial W_{p,q}^{(i)}} W^{(j+1)} \right\|_F^2 \\ &\leq \|P_G\|^2 \|W^{(j+1)}\|^2 \left\| \frac{\partial \psi_{j+1}(H^{(j)})}{\partial W_{p,q}^{(i)}} \right\|_F^2 \\ &\leq \|P_G\|^2 \|W^{(j+1)}\|^2 \left\| \psi'_{j+1}(H^{(j)}) \odot \frac{\partial H^{(j)}}{\partial W_{p,q}^{(i)}} \right\|_F^2 \\ &\leq \kappa_0^2 \|P_G\|^2 \|W^{(j+1)}\|^2 \left\| \frac{\partial H^{(j)}}{\partial W_{p,q}^{(i)}} \right\|_F^2. \end{aligned}$$

Therefore, combining the above with equations (36) together, we get the following result:

$$\begin{aligned} \left\| \frac{\partial^2 H^{(j+1)}}{\partial (W_{p,q}^{(i)})^2} \right\|_F &\leq \left((\kappa_0 + 1) \kappa_0^3 \kappa_1 \|P_G\|^2 \|W^{(j+1)}\|^2 + \kappa_0^2 \kappa_1 \|P_G\| \|W^{(j+1)}\| \right) \left\| \frac{\partial H^{(j)}}{\partial W_{p,q}^{(i)}} \right\|_F^2 \\ &\quad + \kappa_0^3 \|P_G\| \|W^{(j+1)}\| \left\| \frac{\partial^2 H^{(j)}}{\partial (W_{p,q}^{(i)})^2} \right\|_F \\ &\leq \max \left(\|P_G\|, \|P_G\|^2 \right) s_{j+1}^2 \left((\kappa_0^2 + \kappa_0 + 1) \kappa_0^2 \kappa_1 \left\| \frac{\partial H^{(j)}}{\partial W_{p,q}^{(i)}} \right\|_F^2 + \kappa_0^3 \left\| \frac{\partial^2 H^{(j)}}{\partial (W_{p,q}^{(i)})^2} \right\|_F \right). \end{aligned}$$

Based on equation (23) of Proposition (A.7), the first-order derivative of $H^{(j)}$ satisfies:

$$\sum_{p=1}^{d_{i-1}} \sum_{q=1}^{d_i} \left\| \frac{\partial H^{(j)}}{\partial W_{p,q}^{(i)}} \right\|_F^2 \leq \kappa_0^{6(j-i+1)} d_i \|P_G\|^{2(j-i+1)} \|H^{(i-1)}\|^2 \prod_{t=i+1}^j s_t^2. \quad (37)$$

Applying equation (37) to the above (and summing over $p = 1, \dots, d_{i-1}$ and $q = 1, \dots, d_i$) forms

the induction step for showing equation (30):

$$\begin{aligned} \sum_{p=1}^{d_{i-1}} \sum_{q=1}^{d_i} \left\| \frac{\partial^2 H^{(j+1)}}{\partial (W_{p,q}^{(i)})^2} \right\|_F &\leq \frac{\kappa_0^3 - 1}{\kappa_0 - 1} \kappa_0^{6(j-i+1)+2} \kappa_1 d_i \max \left(\|P_G\|^{2(j-i)+3}, \|P_G\|^{2(j-i)+4} \right) \|H^{(i-1)}\|_F^2 \prod_{t=i+1}^{j+1} s_t^2 \\ &\quad + \kappa_0^3 \max (\|P_G\|, \|P_G\|^2) s_{j+1}^2 \sum_{p=1}^{d_{i-1}} \sum_{q=1}^{d_i} \left\| \frac{\partial^2 H^{(j)}}{\partial (W_{p,q}^{(i)})^2} \right\|_F. \end{aligned}$$

By repeatedly applying the induction step along with the base case in equation (34), we have shown that equation (30) holds:

$$\sum_{p=1}^{d_{i-1}} \sum_{q=1}^{d_i} \left\| \frac{\partial^2 H^{(j)}}{(W_{p,q}^{(i)})^2} \right\|_F \leq C_{i,j} \kappa_1 d_i \max (\|P_G\|^{j-i+2}, \|P_G\|^{2(j-i+1)}) \|H^{(i-1)}\|_F^2 \prod_{t=i+1}^j s_t^2, \quad (38)$$

where $C_{i,j}$ satisfies the following equation:

$$C_{i,j} = \begin{cases} \kappa_0^{3(j-i+1)} \frac{\kappa_0^{3(j-i)+2} - 1}{\kappa_0 - 1}, & \kappa_0 \neq 1, \\ 3(j-i) + 2, & \kappa_0 = 1. \end{cases}$$

In the second part of the proof, we consider equation (31) similar to the first part. However, the analysis will be significantly simpler. We first consider the base case. Similar to equation (32), the second-order derivative of $H^{(i)}$ over $W_{p,q}^{(i)}$ satisfies, for any $p = 1, \dots, d_0$ and $q = 1, \dots, d_i$:

$$\left\| \frac{\partial^2 H^{(i)}}{\partial (U_{p,q}^{(i)})^2} \right\|_F = \left\| \phi_i''(E_i) \odot \frac{\partial E_i}{\partial U_{p,q}^{(i)}} \odot \frac{\partial E_i}{\partial U_{p,q}^{(i)}} \right\| \leq \kappa_1 \left\| \frac{\partial (XU^{(i)})}{\partial U_{p,q}^{(i)}} \right\|_F^2.$$

Therefore, by summing up the above over all p and q , we get the base case result:

$$\sum_{p=1}^{d_{i-1}} \sum_{q=1}^{d_i} \left\| \frac{\partial^2 H^{(i)}}{\partial (U_{p,q}^{(i)})^2} \right\|_F \leq \kappa_1 d_i \|X\|_F^2. \quad (39)$$

Next, we consider the induction step from layer j to layer $j+1$. This step follows the same analysis until equation (38), from which we can similarly derive that:

$$\sum_{p=1}^{d_{i-1}} \sum_{q=1}^{d_i} \left\| \frac{\partial^2 H^{(j)}}{(U_{p,q}^{(i)})^2} \right\|_F \leq \hat{C}_{i,j} \kappa_1 d_i \max (\|P_G\|^{j-i}, \|P_G\|^{2(j-i)}) \|X\|_F^2 \prod_{t=i+1}^j s_t^2. \quad (40)$$

where $\hat{C}_{i,j}$ satisfies the following equation:

$$\hat{C}_{i,j} = \begin{cases} \kappa_0^{3(j-i)} \frac{\kappa_0^{3(j-i)+1} - 1}{\kappa_0 - 1}, & \kappa_0 \neq 1, \\ 3(j-i) + 1, & \kappa_0 = 1. \end{cases}$$

A.2.4 Proof of Theorem 3.1

Based on Propositions A.7 and A.8, we are ready to present the proof of Theorem 3.1 for message passing GNNs. First, we will apply the bounds on the derivatives back in Lemma 4.3. After getting the trace of the Hessians, we then use the PAC-Bayes bound from Lemma 4.1 to complete the proof.

Proof of Theorem 3.1. By applying equations (23) and (30) into Lemma 4.3's result, we get that the trace of $\mathbf{H}^{(l)}$ with respect to $W^{(i)}$ is less than:

$$\begin{aligned} & \left(\frac{\kappa_0 \sqrt{k}}{\sqrt{n}} C_{i,l-1} \kappa_1 d_i \max(\|P_G\|^{l-i+1}, \|P_G\|^{2(l-i)}) + \frac{\kappa_1 k}{n} \kappa_0^{6(l-i)} \kappa_1 d_i \|P_G\|^{2(l-i)} \right) \left\| H^{(i-1)} \right\|_F^2 \prod_{t=i+1}^l s_t^2 \\ & \leq (\kappa_0 C_{i,l-1} + \kappa_0^{6(l-i)}) \sqrt{\frac{k}{n}} \kappa_1 d_i \max(\|P_G\|^{l-i+1}, \|P_G\|^{2(l-i)}) \left\| H^{(i-1)} \right\|_F^2 \prod_{t=i+1}^l s_t^2, \end{aligned} \quad (41)$$

for any $i = 1, 2, \dots, l-1$. Here we have

$$\kappa_0 C_{i,l-1} + \kappa_0^{6(l-i)} = \begin{cases} \kappa_0^{3(l-i)+1} \frac{\kappa_0^{3(l-i)} - 1}{\kappa_0 - 1}, & \kappa_0 \neq 1, \\ 3(l-i) - 1, & \kappa_0 = 1. \end{cases}$$

It remains to consider the Frobenius norm of $H^{(i-1)}$. Notice that this satisfies the following:

$$\begin{aligned} \left\| H^{(i-1)} \right\|_F & \leq \kappa_0 \left\| XU^{(i-1)} + \rho_{i-1}(P_G \psi_{i-1}(H^{(i-2)}))W^{(i-1)} \right\|_F \\ & \leq \kappa_0 \left\| U^{(i-1)} \right\| \|X\|_F + \kappa_0^3 \|P_G\| \left\| W^{(i-1)} \right\| \left\| H^{(i-2)} \right\|_F \leq \kappa_0 s_i \|X\|_F + \kappa_0^3 \|P_G\| s_i \left\| H^{(i-2)} \right\|_F. \end{aligned}$$

By induction over i for the above step, we get that the Frobenius norm of $H^{(i-1)}$ must be less than:

$$(\kappa_0^{3(i-1)} + \sum_{j=0}^{i-2} \kappa_0^{3j+1}) \sqrt{k} \max_{(X,G,y) \sim \mathcal{D}} \|X\| \max(1, \|P_G\|^{i-1}) \prod_{j=1}^{i-1} s_j. \quad (42)$$

By applying the above (42) back in (41), we have shown that the trace of $\mathbf{H}^{(l)}$ with respect to $W^{(i)}$ is less than:

$$C' \max_{(X,G,y) \sim \mathcal{D}} \|X\|^2 \kappa_1 d_i k \max(1, \|P_G\|^{2(l-1)}) \prod_{t=1:t \neq i}^l s_t^2, \quad (43)$$

where C' satisfies the following equation:

$$C' = \begin{cases} \frac{(\kappa_0^{3l} - 1)(\kappa_0^{3(l-1)/2} - 1)^2}{(\kappa_0 - 1)^3}, & \kappa_0 \neq 1, \\ \frac{4}{9} l^3, & \kappa_0 = 1. \end{cases}$$

To be specific, when $\kappa_0 = 1$, $(3(l-i) - 1)i^2 \leq \frac{4}{9}l^3$. If $\kappa_0 \neq 1$ and $i \geq 2$, we have

$$\begin{aligned} & \left(\kappa_0^{3(l-i)+1} \frac{\kappa_0^{3(l-i)} - 1}{\kappa_0 - 1} \right) \left(\kappa_0^{3(i-1)} + \sum_{j=0}^{i-2} \kappa_0^{3j+1} \right)^2 \leq \kappa_0^{3(l-i)+3} \frac{\kappa_0^{3(l-i)} - 1}{\kappa_0 - 1} \frac{(\kappa_0^{3(i-1)} - 1)^2}{(\kappa_0 - 1)^2} \\ & = \frac{\kappa_0^{3l} - \kappa_0^{3(l-i+1)}}{(\kappa_0 - 1)^3} \left((\kappa_0^{3(l-i)} - 1)(\kappa_0^{3(i-1)} - 1) \right) \leq \frac{(\kappa_0^{3l} - 1)(\kappa_0^{3(l-1)/2} - 1)^2}{(\kappa_0 - 1)^3}. \end{aligned}$$

If $\kappa_0 \neq 1$ and $i = 1$, we obtain

$$\left(\kappa_0^{3(l-i)+1} \frac{\kappa_0^{3(l-i)} - 1}{\kappa_0 - 1} \right) \left(\kappa_0^{3(i-1)} + \sum_{j=0}^{i-2} \kappa_0^{3j+1} \right)^2 = \kappa_0^{3l-2} \frac{\kappa_0^{3(l-1)} - 1}{\kappa_0 - 1} \leq \frac{(\kappa_0^{3l} - 1)(\kappa_0^{3(l-1)/2} - 1)^2}{(\kappa_0 - 1)^3}.$$

The above works for the layers from the beginning until layer $l - 1$. Last, we consider the trace of $\mathbf{H}^{(l)}$ with respect to $W^{(l)}$ (notice that \mathbf{U} is not needed in the readout layer). Similar to equation (19), one can prove that the trace of the Hessian with respect to $W^{(l)}$ satisfies:

$$\begin{aligned} \left| \text{Tr} [\mathbf{H}^{(l)}[\ell(H^{(l)}, y)]] \right| &\leq \kappa_0 \sqrt{k} \sum_{p=1}^{d_{l-1}} \sum_{q=1}^{d_l} \left\| \frac{\partial^2 H^{(l)}}{\partial (W_{p,q}^{(l)})^2} \right\| + \kappa_1 k \sum_{p=1}^{d_{l-1}} \sum_{q=1}^{d_l} \left\| \frac{\partial H^{(l)}}{\partial W_{p,q}^{(l)}} \right\|^2 \\ &\leq \kappa_0 \sqrt{k} \sum_{p=1}^{d_{l-1}} \sum_{q=1}^{d_l} \left\| \frac{1}{n} \mathbf{1}_n^\top H^{(l-1)} \frac{\partial^2 W^{(l)}}{\partial (W_{p,q}^{(l)})^2} \right\| + \kappa_1 k \sum_{p=1}^{d_{l-1}} \sum_{q=1}^{d_l} \left\| \frac{1}{n} \mathbf{1}_n^\top H^{(l-1)} \frac{\partial W^{(l)}}{\partial W_{p,q}^{(l)}} \right\|^2 \\ &\leq \kappa_1 k \sum_{p=1}^{d_{l-1}} \sum_{q=1}^{d_l} \left\| \frac{1}{n} \mathbf{1}_n \right\|^2 \left\| H^{(l-1)} \frac{\partial W^{(l)}}{\partial W_{p,q}^{(l)}} \right\|^2 \\ &= \kappa_1 \frac{k}{n} d_l \left\| H^{(l-1)} \right\|_F^2 \end{aligned}$$

By equation (42), the above is bounded by

$$\begin{aligned} &\kappa_1 \frac{k}{n} d_l \left(\kappa_0^{3(l-1)} + \sum_{j=0}^{l-2} \kappa_0^{3j+1} \right)^2 \max_{(X, G, y) \sim \mathcal{D}} \|X\|_F^2 \max(1, \|P_G\|^{2(l-1)}) \prod_{j=1}^{l-1} s_j^2 \\ &\leq C_l \max_{(X, G, y) \sim \mathcal{D}} \|X\|^2 \kappa_1 d_l k \max(1, \|P_G\|^{2(l-1)}) \prod_{t=1: t \neq l}^l s_t^2, \end{aligned}$$

since $\frac{\|X\|_F^2}{n} \leq \|X\|^2$, where C_l satisfies the following equation:

$$C_l = \begin{cases} \kappa_0^2 \frac{(\kappa_0^{3(l-1)} - 1)^2}{(\kappa_0 - 1)^2}, & \kappa_0 \neq 1, \\ l^2, & \kappa_0 = 1. \end{cases}$$

Finally, let

$$\tilde{C} = \max(C', C_l). \quad (44)$$

From the value of C' above and the value of C_l , we get that \tilde{C} is equal to

$$\tilde{C} = \begin{cases} \frac{(\kappa_0^{3l} - 1)(\kappa_0^{3(l-1)/2} - 1)^2}{(\kappa_0 - 1)^3}, & \kappa_0 \neq 1, \\ \frac{1}{2} l^3, & \kappa_0 = 1. \end{cases}$$

Similarly by applying equations (24) and (31) into Lemma 4.3, the trace of $\mathbf{H}^{(l)}$ with respect to $U^{(i)}$ is also less than equation (43). Therefore, we have completed the proof for message-passing neural networks.

A.3 Proof of matching lower bound (Theorem 3.2)

For simplicity, we will exhibit the instance for a graph ConvNet, that is, we ignore the parameters in \mathbf{U} and also set the mapping ρ_t and ψ_t as the identity mapping. Further, we set the mapping $\phi_t(x) = x$ as the identity mapping, too, for simplifying the proof. In the proof, we show that for an arbitrary configuration of weight matrices $W^{(1)}, W^{(2)}, \dots, W^{(l)}$, there exists a data distribution such that for this particular configuration, the generation gap with respect to the data distribution satisfies the desired equation (6).

Proof of Theorem 3.2. Recall that the underlying graph for the lower bound instance is a complete graph. Next, we will specify the other parts of the data distribution \mathcal{D} . Let $Z = \prod_{i=1}^l W^{(i)}$ denote the product of the weight matrices. We are going to construct a binary classification problem. Thus, the dimension of Z will be equal to n by 2. Let $Z = UDV^\top$ be the singular value decomposition of Z . Let $\lambda_{\max}(Z)$ be the largest singular value of Z , with corresponding left and right singular vectors u_1 and v_1 , respectively. Within the hypothesis set \mathcal{H} , $\lambda_{\max}(Z)$ can be as large as $\prod_{i=1}^l s_i$. Denote a random draw from \mathcal{D} as X, G, y , corresponding to node features, the graph, and the label:

1. The feature matrix X is equal to $\mathbf{1}_n u_1^\top$;
2. The class label y is drawn uniformly between $+1$ and -1 ;
3. Lastly, the diffusion matrix P is the adjacency matrix of G , which has a value of one in every entry of P .

Given the example and the weight matrices, we will use the logistic loss to evaluate f 's loss. Notice that $P = \mathbf{1}_n \mathbf{1}_n^\top$. Thus, one can verify $\lambda_{\max}(P) = n$. Crucially, the network output of our GCN is equal to

$$H^{(l)} = \frac{1}{n} \mathbf{1}_n^\top P^{l-1} X W^{(1)} W^{(2)} \dots W^{(l)} = n^{l-1} \left(\frac{\mathbf{1}_n^\top X}{n} Z \right) = n^{l-1} \left(u_1^\top UDV^\top \right) = (n^{l-1} \lambda_{\max}(Z)) v_1^\top.$$

Let us denote $\alpha = n^{l-1} \lambda_{\max}(Z)$ —the spectral norms of the diffusion matrix and the layer weight matrices. Let $v_{1,1}, v_{1,2}$ be the first and second coordinate of v_1 , respectively. Notice that y is drawn uniformly between $+1$ or -1 . Thus, with probability $1/2$, the loss of this example is $\log(1 + \exp(-\alpha \cdot v_{1,1}))$; with probability $1/2$, the loss of this example is $\log(1 + \exp(\alpha \cdot v_{1,2}))$. Let b_i be a random variable that indicates the logistic loss of the i -th example. The generalization gap is equal to

$$\epsilon = \frac{1}{N} \sum_{i=1}^N b_i - \frac{1}{2} \left(\log(1 + \exp(-\alpha \cdot v_{1,1})) + \log(1 + \exp(\alpha \cdot v_{1,2})) \right).$$

By the central limit theorem, as N grows to infinity, the generalization gap ϵ converges to a normal random variable whose mean is zero and variance is equal to

$$\frac{1}{4N} \left(\log(1 + \exp(-\alpha \cdot v_{1,1})) - \log(1 + \exp(\alpha \cdot v_{1,2})) \right)^2 \gtrsim \frac{\alpha^2}{N},$$

for large enough values of N . As a result, with probability at least 0.1, when N is large enough, the generalization gap ϵ must be at least

$$O\left(\sqrt{\frac{\alpha^2}{N}}\right), \text{ where } \alpha = \|P_G\|^{l-1} \lambda_{\max}\left(\prod_{i=1}^l W^{(i)}\right).$$

Notice that the product matrix's spectral norm is at most $\prod_{i=1}^l s_i$. Thus, we have completed the proof of equation (6).

A.4 Proof for graph isomorphism networks (Corollary 4.5)

To be precise, we state the loss function for learning graph isomorphism networks as the averaged loss over all the classification layers:

$$\bar{\ell}(f(X, G), y) = \frac{1}{(l-1)} \sum_{i=1}^{l-1} \ell\left(\frac{1}{n} \mathbf{1}_n^\top H^{(i)} V^{(i)}, y\right). \quad (45)$$

Thus, $\hat{L}_{GIN}(f)$ is equivalent to the empirical average of $\bar{\ell}$ over N samples from \mathcal{D} . $L_{GIN}(f)$ is then equivalent to the expectation of $\bar{\ell}$ over a random sample from \mathcal{D} .

Proof of Corollary 4.5. This result follows the trace guarantee from Lemma 4.3. For any $i = 1, \dots, l-1$ and any $j = i, \dots, l-1$, we can derive the following result with similar arguments:

$$\left| \text{Tr} \left[\mathbf{H}_W^{(i)} \left[\ell \left(\frac{1}{n} \mathbf{1}_n^\top H^{(j)} V^{(j)}, y \right) \right] \right] \right| \leq \frac{\kappa_0 \sqrt{k}}{\sqrt{n}} \|V^{(j)}\| \sum_{p=1}^{d_{i-1}} \sum_{q=1}^{d_i} \left\| \frac{\partial^2 H^{(j)}}{\partial (W_{p,q}^{(i)})^2} \right\|_F + \frac{\kappa_1 k}{n} \|V^{(j)}\|^2 \left\| \frac{\partial H^{(j)}}{\partial W^{(i)}} \right\|_F^2.$$

Next, we repeat the steps in Propositions A.7 and A.8, for any $i = 1, \dots, l-1$ and any $j = i, \dots, l-1$:

$$\begin{aligned} & \max_{(X, G, y) \sim \mathcal{D}} \left| \text{Tr} \left[\mathbf{H}^{(i)} \left[\ell \left(\frac{1}{n} \mathbf{1}_n^\top H^{(j)} V^{(j)}, y \right) \right] \right] \right| \\ & \leq 2\kappa_1 \tilde{C} d_i k \max_{(X, G, y) \sim \mathcal{D}} \|X\|^2 \max \left(1, \|P_G\|^{2(j-i+1)} \right) \|V^{(j)}\|^2 \prod_{t=1: t \neq i}^j s_t^2. \end{aligned}$$

Based on the above step, the trace of the loss Hessian matrix with respect to $W^{(i)}, U^{(i)}$ satisfies:

$$\begin{aligned} & \max_{(X, G, y) \sim \mathcal{D}} \left| \text{Tr} \left[\mathbf{H}^{(i)} \left[\bar{\ell}(f(X, G), y) \right] \right] \right| \\ & = \max_{(X, G, y) \sim \mathcal{D}} \left| \text{Tr} \left[\mathbf{H}^{(i)} \left[\frac{1}{(l-1)} \sum_{j=1}^{l-1} \ell \left(\frac{1}{n} \mathbf{1}_n^\top H^{(j)} V^{(j)}, y \right) \right] \right] \right| \\ & = \frac{1}{l-1} \sum_{j=i}^{l-1} \max_{(X, G, y) \sim \mathcal{D}} \left| \text{Tr} \left[\mathbf{H}^{(i)} \left[\ell \left(\frac{1}{n} \mathbf{1}_n^\top H^{(j)} V^{(j)}, y \right) \right] \right] \right| \\ & \leq 2\kappa_1 \tilde{C} d_i k \max_{j=1}^{l-1} \|V^{(j)}\|^2 \left(\max_{(X, G, y) \sim \mathcal{D}} \|X\|^2 \sum_{j=1}^{l-1} \frac{\max(1, \|P_G\|^{2j})}{l-1} \right) \prod_{t=1: t \neq i}^{l-1} s_t^2. \end{aligned}$$

Within the above step, the propagation matrix satisfies:

$$\frac{1}{(l-1)} \sum_{j=1}^{l-1} \max(1, \|P_G\|^{2j}) \leq \max \left(1, \left\| \frac{1}{l-1} \sum_{j=1}^{l-1} P_G^j \right\|^2 \right).$$

Notice that $P_{GIN} = \frac{1}{l-1} \sum_{j=1}^{l-1} P_G^j$. Thus, we have completed the generalization error analysis for graph isomorphism networks in equation (11).

B Experiment Details

For our result, we measure B as an upper bound on the loss value taken over the entire data distribution. Across five datasets in our experiments, setting $B = 5.4$ suffices for all the training and testing examples in the datasets.

For comparing generalization bounds, we use two types of model architectures, including GCN [36] and the MPGNN in Liao et al. [38]. Following the setup in Liao et al. [38], we apply the same network weights across multiple layers in one model, i.e., $W^{(t)} = W$ and $U^{(t)} = U$ across the first $l - 1$ layers. For GCNs, we set \mathbf{U} as zero, ρ_t and ψ_t as identity mappings, ϕ_t as ReLU function. For MPGNNs, we specify ϕ_t as ReLU, ρ_t and ψ_t as Tanh function. For both model architectures, we set the width of each layer $d_t = 128$ and vary the network depth l in 2, 4, and 6. On the three collaboration network datasets, we use one-hot encodings of node degrees as input node features. We train the models with Adam optimizer with a learning rate of 0.01 and set the number of epochs as 50 and batch size as 128 on all three datasets. We compute the generalization bounds following the setup in Liao et al. [38]. Theorem 3.4 from Liao et al. [38]:

$$\sqrt{\frac{42^2}{\gamma^2 N} \left(\max_{(X, G, y) \sim \mathcal{D}} \|X\|^2 \right) \left(\max \left(\zeta^{-l+1}, (\lambda \xi)^{\frac{l-1}{2}} \right) \right)^2 l^2 h \log(4lh)(2s_1^2 r_1^2 + s_l^2 r_l^2)},$$

where $\zeta = \min(s_1, s_l)$, $\lambda = s_1 s_l$, $\xi = \frac{(ds_1)^{l-1}-1}{ds_1-1}$, d is the max degree, h is the max hidden width, and γ is the desired margin in the margin loss. Note that $s_i = s_1$ and $r_i = r_1$ for $1 \leq i \leq l - 1$ since the first $l - 1$ layers apply the same weight. Proposition 7 from Garg et al. [16]:

$$48s_l h Z \sqrt{\frac{3}{\gamma^2 N} \log(24s_l \sqrt{N} \max(Z, M\sqrt{h} \max(\kappa_2 s_1, \bar{R}s_1)))},$$

where $M = \frac{(ds_1)^{l-1}-1}{ds_1-1}$, $\bar{R} = d \cdot \min(\kappa_1 \sqrt{h}, \kappa_2 s_1 M)$, $Z = \kappa_2 s_1 + \bar{R}s_1$, $\kappa_1 = \max_{x \in \mathbb{R}^h} \|\phi(x)\|_\infty$, and $\kappa_2 = \max_{(X, G, y) \sim \mathcal{D}} \|X\|^2$.